Global and Planetary Change 227 (2023) 104153

Contents lists available at ScienceDirect

Global and Planetary Change

journal homepage: www.elsevier.com/locate/gloplacha

Macroevolutionary and macroecological response of Iberian rodents to late Neogene climatic oscillations and events

Jan A. van Dam [a,b,*], Pierre Mein [c], Miguel Garcés [d], Ronald T. van Balen [e,f], Marc Furió [b,g], Luis Alcalá [h]

[a] Department of Earth Sciences, Utrecht University, Vening Meinesz Building A, Princetonlaan 8a, 3584 CB Utrecht, the Netherlands
[b] Institut Català de Paleontologia Miquel Crusafont, c/ Columnes s/n Campus de la UAB 08193, Cerdanyola del Vallès, Barcelona, Spain
[c] A.R.P.A Université Lyon 1, Bâtiment Géode 69622, Villeurbanne Cedex, France
[d] Departamento de Dinàmica de la Terra i de l'Oceà, Facultat de Ciències de la Terra, Universitat de Barcelona, Barcelona, Spain
[e] Department of Earth Sciences, Vrije Universiteit Amsterdam, De Boelelaan 1085, 1081 HV Amsterdam, the Netherlands
[f] TNO-Geological Survey of the Netherlands, Princetonlaan 6, 3584 CB Utrecht, the Netherlands.
[g] Serra Húnter Fellow, Universitat Autònoma de Barcelona, Geology Department, Cerdanyola del Vallès (08193), Barcelona, Spain.
[h] Parque de las Ciencias de Andalucía, Av. de la Ciencia, s/n, Granada (18006), Spain.

ARTICLE INFO

Editor: Dr. Howard Falcon-Lang

Keywords:
Neogene
Spain
Rodentia
Climate
Precipitation
Milankovitch cycles
Macroevolution
Macroecology
Migration
Clade replacement

ABSTRACT

Biozones are routinely used for chronological purposes, but their nature is seldomly questioned. Here, we attempt to find the evolutionary-ecological basis for Iberian rodent biozones for the interval 8.5–2 Ma based on currently available paleontological, stratigraphic and paleoclimatic information. Our comparison of biozone boundary age uncertainty intervals to records of marine SST, $\delta^{18}O$ and $\delta^{13}C$, terrestrial hydrological proxies and astronomical parameters suggests an orbitally forced climatic origin for the majority of biozones. Zone boundary ages during the late Miocene are mostly associated with humidity changes during 1.2-Myr obliquity nodes and 405-kyr eccentricity minima. Tectonics and strong regional cooling may additionally explain faunal change during the Messinian (7–5 Ma). A partly reversed pattern characterizes most Pliocene zone boundaries, which are mostly associated with wetter conditions during obliquity nodes and 405-kyr eccentricity maxima. A third configuration culminates in the early Pleistocene and consists of the combination of strong obliquity amplitude maxima and 2.4-Myr eccentricity minima. It is suggested that larger-scale, European Neogene mammal (MN) units have an astronomical basis as well, with an important role of 2.4-Myr eccentricity cycle and the 1.2-Myr obliquity cycle, with the latter becoming especially important after the mid-Miocene cooling (~14 Ma).

Whereas rodent events on the Iberian Peninsula during the late Miocene are shaped by replacements within resident communities dominated by dry-adapted clades of true mice (Murinae) and hamsters (Cricetinae), transitions during the cooler Pliocene involve invasions of newly emerging Eurasian clades of 'microtoid hamsters' and voles (Arvicolinae) preferring wetter and cooler environments. A new model of stepwise clade displacement is proposed in which the combination of long-period Milankovitch cycles and gradual long-term climatic change allows for the periodic functioning of migration corridors, along which increasingly pervasive dispersal events by members of new clades cause the gradual extinction of old clades.

1. Introduction

Since long, stratigraphers have been using biozones for correlating sediments across a wide range of temporal and spatial scales. The evolutionary-ecological basis of such zones is often not well understood, however. To comprehend the observed persistence of relatively fixed sets of taxa over very long periods, insight is required into the long-term processes that control ecological communities (macroecology) and into the biotic and abiotic factors that trigger species extinction, origination and migration (macroevolution; Vrba, 1995; Barnosky, 2001; Fraser et al., 2021). Apart from tectonic or eustatic sea-level events that occasionally lead to openings or closures of migration routes between formerly separated (sub-)continents, climatic events would be among the first to be held responsible for controlling million year-scale faunal

* Corresponding author at: Department of Earth Sciences, Utrecht University, Vening Meinesz Building A, Princetonlaan 8a, 3584 CB Utrecht, the Netherlands.
E-mail address: j.a.vandam@uu.nl (J.A. van Dam).

https://doi.org/10.1016/j.gloplacha.2023.104153
Received 13 February 2023; Received in revised form 16 May 2023; Accepted 18 May 2023
Available online 24 May 2023

dynamics.

Rodents are the most important organisms for subdividing Cenozoic continental stratigraphy. Their rapid evolution has helped geologists to define local biozones with durations in the order of several hundred thousands of years at the local basin scale (van de Weerd, 1976; Kälin and Kempf, 2009; van der Meulen et al., 1999) and bioprovincial scale (van Dam et al., 2023) to 1–2 Myr at the continental scale (Mein, 1990; Hilgen et al., 2012; Speijer et al., 2020). With abiotic factors, such as climate change, and biotic factors, such as competition, continuously affecting communities at ecological time scales, biozone-scale community stasis should be qualified as a remarkable phenomenon that deserves an explanation (Ivany, 1996).

In a previous analysis covering a large part of the Neogene, we found support for a climatic mechanism explaining the million-year scale clustering of rodent turnover, with faunal change being concentrated during low-amplitude intervals (nodes) of the Earth's Milankovitch cycles of eccentricity and/or obliquity (2.4-Myr and 1.2-Myr cycles; van Dam et al., 2006). In that study, which was based on records from central Spain, increased turnover during such nodes was hypothesized to work in two ways: 1) remotely, via high-latitude global cooling events and their global effects, and 2) locally/regionally, via the breaking down of the 'regular' evolutionary-ecological response to short-period cycles (i.e., short-distance migration and re-assembly of incipient species with mother species).

To study the response to medium-period cycles such as the ~100-kyr and 405-kyr eccentricity cycles, a high temporal resolution of fossil localities is indispensable. Furthermore, to better understand the spatial dimension of macroevolutionary and macroecological processes, the inclusion of a geographical component is highly desirable. Here, we focus on the climatically dynamic late Miocene to early Pleistocene (8.5–2 Ma), studying rodent communities from a series of Iberian basins (Fig. 1), for several of which new rodent and chronological data have recently become available. Our recent revision of all paleontological and stratigraphic evidence (van Dam et al., 2023) has resulted in the formulation of an overarching, Iberian-scale rodent stratigraphic framework (Table 1), on the basis of which the age accuracy of many sites could be increased.

In this study we use species relative abundances (molar frequencies) for reconstructing both temporal and geographical gradients in community structure. Focusing on the dominant family of Muridae, our analysis of these gradients leads to a better understanding of patterns of migration and evolution and their combined effect during 'clade replacement' (the substitution of one higher taxonomic unit by another, e.g., Benton, 1996; Fraser et al., 2021).

2. Material and methods

2.1. Chronology

Age uncertainty ranges for Iberian assemblage biozone boundaries and individual mammal sites are taken from van Dam et al. (2023), who combined Iberian rodent biostratigraphy with local magnetostratigraphy and interpolations based on sedimentation and/or evolutionary rates (Table 1). Iberian rodent biozones are coded by 'Ib-N' (Iberian Neogene) and followed by a number (11, 12, etc.) that roughly corresponds to the time-equivalent MN unit, and a letter to indicate the actual Zone (Ib-N12a, Ib-N12b, etc.). All paleontological and climatic records included in this paper are calibrated to the newest Geomagnetic Polarity Time Scale (GPTS; Raffi et al., 2020), which, in turn, is calibrated to the Astronomical Time Scale (ATS; Laskar et al., 2004; Hilgen et al., 2020).

2.2. Relative abundances

Relative abundances for 27 murid lineages consisting of true mice (Murinae), hamsters (Cricetinae, Cricetodontinae), vole-like hamsters (Baranomyinae, Trilophomyinae), and voles (Arvicolinae) were compiled per locality and per zone. Several rare lineages and

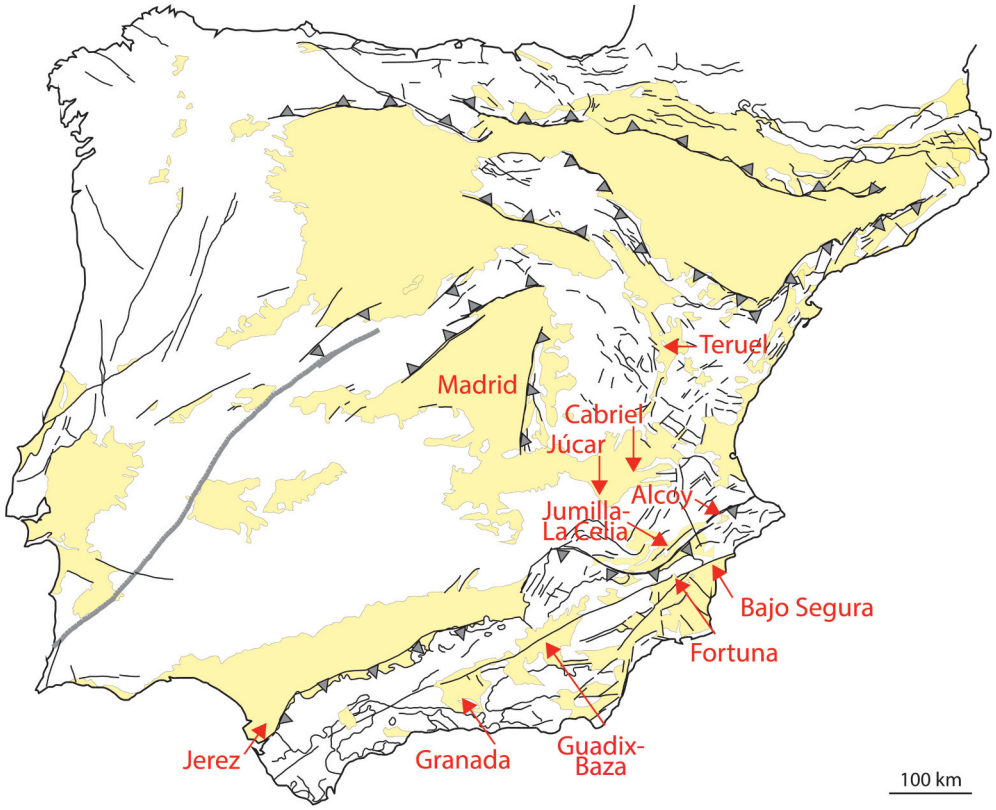

Fig. 1. Map of the Iberian Peninsula with Cenozoic basins used in this study.

Table 1
Iberian rodent zones with boundaries and ages (after van Dam et al., 2023).

Iberian Assemblage Zone		Zone boundary	Age (Ma)			Duration (Myr)	Age (Ma)	Duration (Myr)
Name	Code		Maximum	Minimum	Midpoint	Uncertainty	Midpoint	Average
		top Ib-N17b	1.90	1.80	1.85	0.10		
Mimomys realensis	Ib-N17b						1.98	0.25
		Ib-N17a-b	2.15	2.05	2.10	0.10		
Mimomys medasensis	Ib-N17a						2.33	0.45
		Ib-N16b-17a	2.56	2.54	2.55	0.02		
Kislangia ischus	Ib-N16b						2.80	0.50
		Ib-N16a-b	3.06	3.03	3.05	0.03		
Mimomys hassiacus	Ib-N16a						3.12	0.14
		Ib-N15b-16a	3.19	3.18	3.19	0.01		
Dolomys adroveri	Ib-N15b						3.58	0.78
		Ib-N15a-b	4.01	3.92	3.97	0.09		
Mimomys davakosi	Ib-N15a						4.10	0.27
		Ib-N14c-15a	4.27	4.19	4.23	0.08		
Trilophomys castroi	Ib-N14c						4.42	0.38
		Ib-N14b-c	4.71	4.51	4.61	0.20		
Paraethomys baeticus	Ib-N14b						4.75	0.28
		Ib-N14a-b	4.91	4.87	4.89	0.04		
Apocricetus barrierei	Ib-N14a						5.15	0.51
		Ib-N13c-14a	5.47	5.33	5.40	0.14		
Paraethomys meini	Ib-N13c						5.83	0.86
		Ib-N13b-c	6.26	6.25	6.26	0.01		
Apocricetus alberti	Ib-N13b						6.34	0.16
		Ib-N13a-b	6.56	6.27	6.42	0.29		
Castromys inflatus	Ib-N13a						6.69	0.55
		Ib-N12b-13a	7.02	6.90	6.96	0.12		
Parapodemus meini	Ib-N12b						7.05	0.18
		Ib-N12a-b	7.18	7.09	7.14	0.09		
Huerzelerimys turoliensis	Ib-N12a						7.40	0.53
		Ib-N11-12a	7.68	7.65	7.67	0.03		
Huerzelerimys vireti	Ib-N11						8.18	1.03
		base Ib-N11	8.75	8.63	8.69	0.12		

unidentified forms not assignable to any of the main lineages were combined with jumping mice, gerbils and myocricetodontines into a single rest group (Muridae plus Dipodidae rest group). The remaining taxa (Sciuridae, Gliridae, Castoridae, Hystricidae) were aggregated into a second rest group. Abundances were based the total number of molars (M/m123). In case only counts of measurable specimens were available from the literature, those counts were used as an alternative for total counts. Abundance data were restricted to zones or localities with $n \geq 25$ specimens and to localities with age uncertainties $\leq$200 kyr.

2.3. Precipitation and lake level proxies

We used the Climate-Diversity Approach of van Dam (2006) and van Dam and Utescher (2016) to predict precipitation levels. The following equations for mean annual precipitation (MAP) and driest- and wettest-month precipitation (LMP, HMP) were used:

$$\mathrm{MAP} = 9.466 + 45.119\ ln^2(\mathrm{PA}+1) + 12.743\ \mathrm{PI} \quad (1)$$

$$\left(R^2 = 0.83\right)$$

$$\mathrm{LMP} = 1.689 + 10.801\ ln(\mathrm{PA}+1) \quad (2)$$

$$\left(R^2 = 0.79\right)$$

$$\mathrm{HMP} = 8.108 + 1.674\ ln^3(\mathrm{PA}+1) + 1.896\ \mathrm{PI} \quad (3)$$

$$\left(R^2 = 0.74\right)$$

with

PA = percentage of arboreal species in the non-aerial, non-(semi) aquatic micromammal community (rodents, eulipotyphlans, lagomorphs).

PI = percentage of invertivorous species (species dominantly consuming invertebrate prey) in the same micromammal community.

Eq. (2) differs slightly from the one published by van Dam and Utescher (2016), which contains a minor error (resulting in a difference of maximally 1.5 mm). A second modification regarding the latter work concerns the ecology of the squirrel genus *Csakvaromys* (which includes '*Spermophilinus*'; Sinitsa et al., 2022) for which we assume an arboreal way of life based on a study of its microwear and cranial shape (laterally directed orbits; Gusovsky and Sinitsa, 2021; Sinitsa et al., 2022).

Prediction intervals for individual sites typically are ±350, ±20, and ± 60 mm wide for MAP, LMP and HMP, respectively (van Dam and Utescher, 2016). 100 specimens was taken as a minimum for Eqs. (1)–(3) to be applied. In the absence of quantitative information on eulipotyphlans and lagomorphs, a minimum of 70 rodent specimens was used for a locality to be included (85 in case one group was missing). In the total absence of any frequency data, we considered 10 species as the minimum for a locality to be included. Because the lagomorph material of some localities has sometimes remained unstudied, we used the lagomorph species richness and micromammal specimen counts of time-equivalent localities to approximate the number of lagomorph species as follows (with n_{R+Li} = number of rodent plus lipotyphlan specimens): one ochotonid species if $n_{R+Li} \geq 10$, one leporid species in Ib-N14a-15b if $n_{R+Li} \geq 100$ and in Ib-N16a-17b if $n_{R+Li} \geq 10$, and zero leporid species in Ib-N13c or lower (unless reported). Furthermore, unidentified (indet.) Eulipotyphla, Soricidae, Talpidae, Sciuridae were assumed to be terrestrial, Arvicolinae and *Mimomys* indet. were assumed to be terrestrial up and including Zone Ib-N15a, and (semi-)aquatic for Zones Ib-N15b-17b.

The proportion f(aq) of (semi-) aquatic micromammal species in the fauna (beavers, watermoles, aquatic shrews and water voles) was used as a proxy for the presence of water bodies. We note that the extrapolation of a semi-aquatic lifestyle of several modern voles (*Arvicola*, *Ondatra*) to their supposed Pliocene relatives (*Mimomys hassiacus - M. pliocaenicus, M. medasensis and Dolomys*) is hypothetical, although generally agreed upon by specialists (see van Dam, 2006). A second,

more qualitative hydrological indicator consists of the stratigraphic distribution of lacustrine/palustrine facies complexes (presence of carbonate/marl lithologies) in the Teruel Basin, where the sedimentary record is the most complete.

3. Results

3.1. Relative abundance trends and gradients

3.1.1. Zone-level comparisons

Lineage relative abundances per zone and region are shown in Fig. 2A (data in Table S1). Three major patterns can be discerned:

1) A dominance shift from Murinae and Cricetinae in the late Miocene to vole-like hamsters (Baranomyinae, Trilophomyinae) and Arvicolinae in the Pliocene and Early Pleistocene.
2) An exclusive presence or a presence with larger abundances of new lineages in the North (i.e., Central Spain) compared to the South. This pattern applies to *Stephanomys* in Ib-N13a, *Blancomys sanzi* in Ib-N13a, *Celadensia* in Ib-N14a, *Promimomys* in Ib-N14b, *Trilophomys* from Ib-N14c onwards, *Mimomys davakosi* in Ib-N15a, *M. gracilis* in Ib-N15b, *M. hassiacus* in Ib-N16a, and *Kislangia ischus* in Ib-N16a. An exception is the arvicoline *Dolomys adroveri* in Ib-N15b, which has a slightly larger proportion in the South (Guadix-Baza Basin) than in the North (Teruel Basin). On the other hand, the scarcity of arvicolines in the same zone in the Jerez Basin, the most south-western region in this study for which there are data, confirms the overall pattern. Superposed on the latitudinal pattern is a temporal pattern with younger immigrants such as *Trilophomys*, but especially *Dolomys*, *Mimomys* and *Kislangia* penetrating further south into the Peninsula than older immigrants such as *Blancomys sanzi*, *Celadensia* and *Promimomys*, which fail to colonize the South. As a net result, the quantitative replacement in the South of the older true mouse and hamster clades by the vole-like and vole clades lags the equivalent replacement in the north by several millions of years (Fig. 2B, Table S2).
3) A late Miocene east-west gradient in true mice versus hamsters. Whereas the former are more abundant in the north (Teruel and Madrid Basins) and extreme south (Granada Basin), the latter are especially abundant in the east (Bajo Segura, Cabriel and Alcoy Basins Basin). This eastern part also functions as the major colonization area for the murine *Paraethomys*, which is regarded as an African immigrant.

3.1.2. Locality-level comparisons

At the locality level, the following patterns can be noted (Fig. 2C):

1) The most important abundance changes occur at boundaries. As a result, lineages may show high and relatively constant abundance levels across a specific zone, and much lower levels below and above it (Fig. 2C: left part). For example, *Castillomys* shows a more or less constant level of temporary raised abundances in the Teruel Basin during Zone Ib-N15b. Similarly, although it is relatively rare, *Blancomys* has its maximum abundance in Ib-N16a. Comparable examples from the Bajo Segura Basin include *Cricetulodon lucentensis* across Ib-N12a, *Neocricetodon* across Ib-N13a, and the *Parapodemus barbarae – P. meini – Castromys* lineage across both zones (Fig. 2C).
2) Peak events involving abundances as high as 70–80% at the base of a zone, followed by a decline (Fig. 2C: upper right part). Examples are *Mimomys davakosi*, *Dolomys adroveri* and *M. hassiacus* in the Teruel Basin.
3) Occasionally, even more extreme peak events occur during which a sudden abundance change is immediately neutralized. Examples are short-lasting maxima of *Parapodemus gaudryi* (Fig. 2C: lower right part) and *Apocricetus* aff. *plinii* at the Ib-N11-12a boundary in the Bajo Segura Basin (Crevillente 4; de Bruijn et al., 1975; van Dam et al., 2023). Similar peak-like occurrences of *Apocricetus* occur in Ib-N13a and 13c at 6.6 and 6.0 Ma (Crevillente 14 and 6; Freudenthal et al., 1998).

3.2. Precipitation and lake level

Precipitation predictions were inferred for 78 localities resulting in mean values of 380, 9 and 59 mm for MAP, LMP and HMP, respectively (Fig. 3D; Table S3). Highest average and wettest-month values (MAP = 831, HMP = 114 mm) were estimated for Concud 3 (Ib-N12a, Teruel Basin, Central Spain). A driest-month maximum was recorded for Crevillente 8 (Ib-N12a, Bajo Segura Basin, LMP = 34 mm). Very dry annual estimates of only ~10 mm/yr were estimated for several southeastern Ib-N13a-14c localities in the Fortuna Basin (Sifón de Librilla 1, 61, 413 and P), Cabriel Basin (La Bullana 2B, Fuente del Viso), Granada Basin (La Mina 2) and Guadix-Baza Basin (Gorafe 4/A). These extreme values, which would point to truly desertic conditions, are a direct reflection of the absence of (insectivorous) eulipotyphlans (PI = 0; Eq. (1)), a group with standard presence in Iberian micromammal faunas. Our method is effectively breaking down for these sites with MAP/12 values exceeding HMP estimates (Table S3). This discrepancy occurs, because even the driest Sahara desert sites in the modern calibration data set for Eqs. (1)–(3) have at least one eulipotyphlan species present (van Dam, 2006). Regardless of the possible existence of some sort of taphonomic bias against eulipotyphlans, it is safe to say that eastern/southern Spain was occasionally extremely arid during the latest Miocene to earliest Pliocene. Even today, this area is the driest part of the Iberian Peninsula (e.g., Tabernas Desert; province of Almeria).

The overall trend in precipitation consists of a gradual decrease from the late Miocene to early Pleistocene, with a distinct maximum occurring during Ib-N12a (7.65–7.15 Ma) and smaller maxima concentrated around the Ib-N14a-b boundary and during Ib-N15a and 16a (Fig. 3C). In addition, a trend towards seasonally more homogeneous levels characterizes Ib-N15b. Maxima in the occurrence of lacustrine/palustrine sediments in the Teruel Basin (indicating lake level, Fig. 3F) are approximately coeval with precipitation maxima.

4. Discussion: The origin of rodent zones

Our search for mechanisms behind rodent zone transitions primarily consists of a systematic investigation of time-correlative and potentially perturbing extrinsic events. Three types of events are chronologically explored: 1) high-latitude climatic events as reflected in North Atlantic $\delta^{18}O$ and sea-surface temperature (SST) records (ODP drilling sites), 2) regional, mid-latitude/Mediterranean climate- and tectonics related events as observed in marine $\delta^{18}O$, $\delta^{13}C$ and SST records and terrestrial hydrological proxy records, 3) critical climatic episodes as predicted from astronomical parameters (eccentricity/precession and obliquity). These chronological explorations will be followed by a summary of those events that most successfully predict faunal change across zone transitions. The section finishes with the formulation of a new model of clade displacement and a discussion on the origin of European-scale mammal chronological (MN) units.

4.1. High-latitude climatic events

The Ib-N11/12a transition between 7.68 and 7.65 Ma is not associated with any distinct positive oceanic benthic $\delta^{18}O$ excursion (cooling/glaciation) event in the NE Atlantic (Fig. 3B) or more distant regions (e.g., equatorial Atlantic and Pacific sites ODP-926 and IODP-U1337; Shackleton and Hall, 1997; Drury et al., 2017). Alkenone-based SST records do show some cooling, however, with values starting to drop at ~7.9 Ma at site ODP-982 and culminating in two small cooling peaks at 7.57 and 7.52 Ma (Fig. 3A). A prominent positive benthic $\delta^{18}O$ excursion of ~0.5‰ at 7.56 Ma ± 0.04 Myr was nevertheless reported in the southeastern Atlantic (ODP-1085; Westerhold et al., 2005). In turn, this

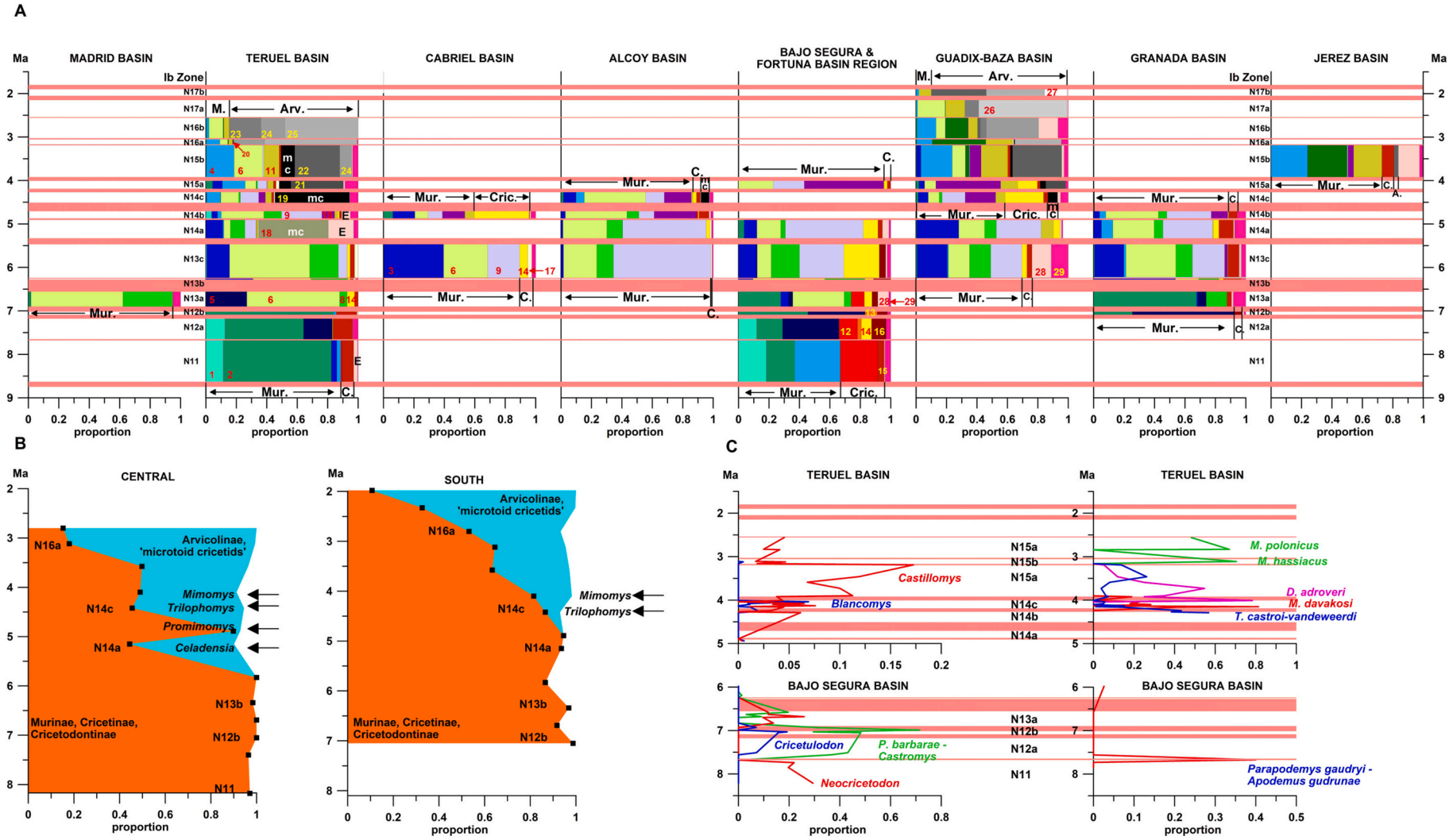

Fig. 2. Rodent relative abundance patterns. (A) Lineage patterns per basin and per Ib Zone (Ib-N11-N17b, specimen $n \geq 25$); long red bars: zone boundary uncertainty intervals; blue, green and purple colors: true mice (Mur., M. = Murinae; lineages 1–11); red, yellow and brown colors: hamsters (Cric., C. = Cricetinae/Cricetodontinae; lineages 12–17); khaki and black colors: vole-like hamsters (mc = 'microtoid cricetids'; lineages 18–20); grey and white colors: voles (Arv., A. = Arvicolinae; lineages 21–27); pink colors: rest groups (28–29). Individual lineages: 1) *Huerzelerimys vireti - H. turoliensis*, 2) *Progonomys hispanicus – Occitanomys sondaari – O. adroveri - O. brailloni*, 3) *Parapodemus gaudryi – Apodemus gudrunae – A. gorafensis*, 4) *Parapodemus lugdunensis - Apodemus atavus*, 5) *Parapodemus barbarae - P. meini - Castromys juniensis - C. littoralis - C. inflatus*, 6) *Stephanomys ramblensis – S. dubari – S. cordii – S. margaritae – S. vandeweerdi – S. minor – S. prietaensis – S. balcellsi – S. progressus*, 7) *Stephanomys donnezani - S. thaleri*, 8) *Occitanomys alcalai*, 9) *Paraethomys meini*, 10) *Paraethomys baeticus - P. abaigari - P.* aff. *jaegeri - P. jaegeri*, 11) *Castillomys gracilis – C. crusafonti – C. rivas*, 12) *Neocricetodon occidentalis - N. seseae*, 13) *Cricetulodon meini - C. lucentensis*, 14) *Apocricetus* aff. *plinii - A. plinii - A. alberti - A. barrierei - A. angustidens*, 15) *Hispanomys aragonensis - H. peralensis – H. freudenthali – Ruscinomys schaubi – R. lasallei – R. europaeus*, 16) *Hispanomys adroveri - H.* aff. *adroveri - H. romeroi, 17) Blancomys sanzi - B. neglectus - B. meini*, 18) *Celadensia nicolae*, 19) *Trilophomys castroi - T. vandeweerdi*, 20) *Trilophomys depereti - T.* sp. A., 21) *Mimomys davakosi*, 22) *Dolomys adroveri - Kislangia cappettai - K.* aff. *cappettai*, 23) *Kislangia ischus - K. gusii*, 24) *Mimomys gracilis - M. stehlini*, 25) *Mimomys hassiacus - M. polonicus - M. praepliocaenicus - M. pliocaenicus*, 26) *Mimomys medasensis*, 27) *Mimomys realensis.* Rest groups: 28) remaining lineages in Muridae and Dipodidae, E = *Eozapus*, 29) remaining lineages in Castoridae, Gliridae, Hystricidae and Sciuridae. For data see Table S1. (B) Trends in the proportion of 'old clades' (Murinae, Cricetinae, Cricetodontinae) versus 'new clades' ('microtoid cricetids', Arvicolinae) in central Spain (Teruel Basin) and southern Spain (Granada and Guadix-Baza Basins); black squares represent zone averages, with values for southern Spain representing average proportions for the two basins; localities with ambiguous zone assignment are excluded. For data see Table S2. (C) Trends for selected taxa (see text); included are sites with $n \geq 25$ and age uncertainty ≤200 kyr; red bars represent zone boundary uncertainty intervals. For data see van Dam et al. (2023). (For interpretation of the references to colour in this figure legend, the reader is referred to the web version of this article.)

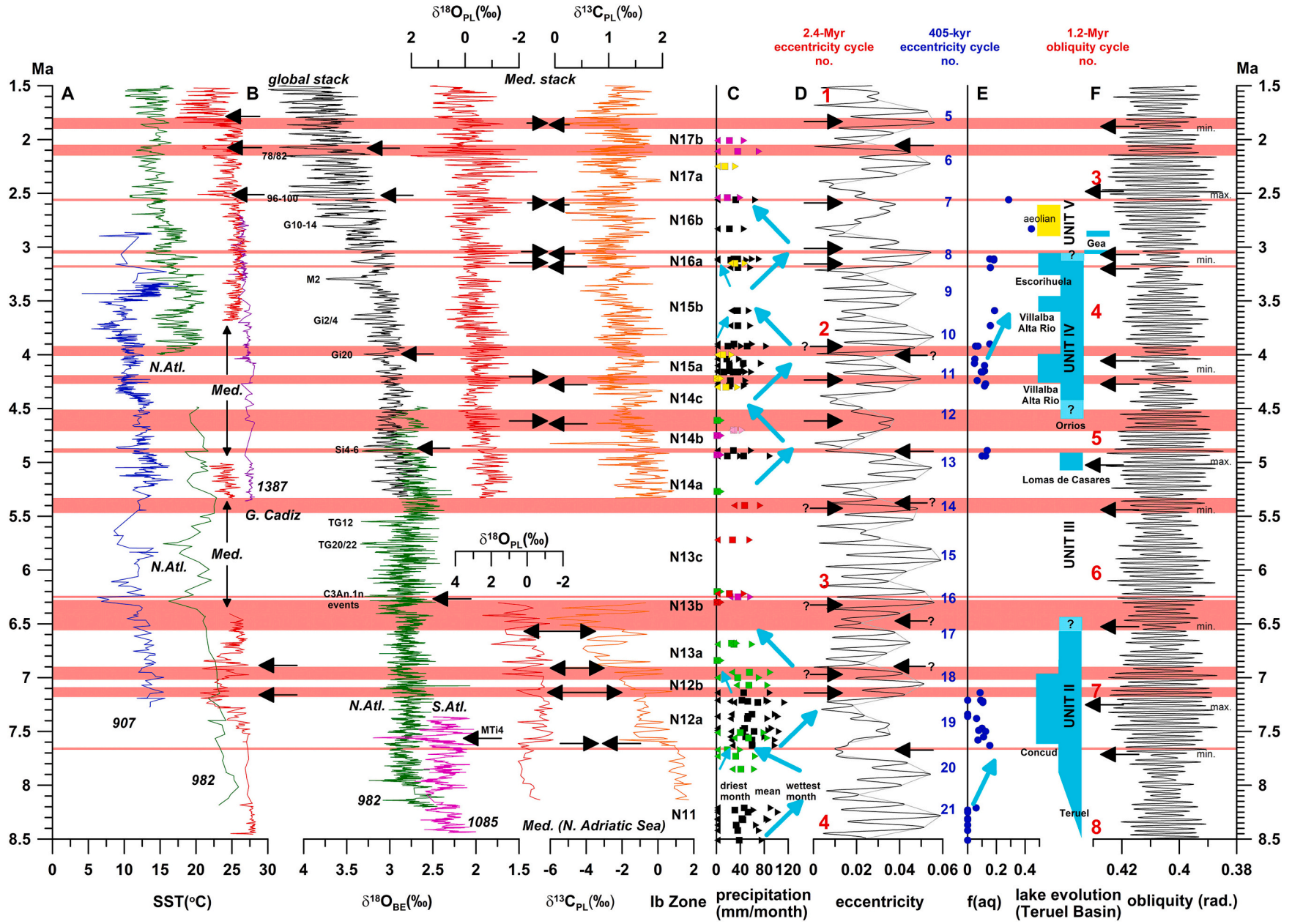
δ18OPL(‰)
δ13CPL(‰)
Med. stack
2.4-Myr eccentricity cycle no.
405-kyr eccentricity cycle no.
1.2-Myr obliquity cycle no.
Ma
A
B
C
D
E
F
global stack
78/82
96-100
G10-14
M2
Gi2/4
Gi20
Si4-6
TG12
TG20/22
C3An.1n events
MTi4
N.Atl.
S.Atl.
Med.
1387
G. Cadiz
907
982
1085
Med. (N. Adriatic Sea)
N17b
N17a
N16b
N16a
N15b
N15a
N14c
N14b
N14a
N13c
N13b
N13a
N12b
N12a
N11
driest month
mean
wettest month
aeolian
Gea
Escorihuela
Villalba Alta Rio
Orrios
Lomas de Casares
Concud
Teruel
UNIT V
UNIT IV
UNIT III
UNIT II
min.
max.
SST(°C)
δ18OBE(‰)
δ13CPL(‰)
Ib Zone
precipitation (mm/month)
eccentricity
f(aq)
lake evolution (Teruel Basin)
obliquity (rad.)

Fig. 3. Correlation diagram of Ib-N Zone boundaries with Mediterranean and Atlantic climate records, estimated precipitation (Spain), proportions (semi-)aquatic species and major sedimentary units (Teruel Basin), and orbital parameters (eccentricity, obliquity). Horizontal red bars: zone boundary uncertainty ranges, horizontal black arrows: important events that correlate to zone boundaries (see text). (A) Alkenone (U^k37)-based SST records from N. Atlantic (ODP-907, 982, 1387) and Mediterranean (Herbert et al., 2016; Tzanova et al., 2015; Tzanova and Herbert, 2015) re-calibrated according to Conte et al. (2006) and with re-calibrated chronology by Lawrence et al. (2009) and Drury et al. (2017) (ODP-982) and by van der Schee et al. (2016) (IODP-1387, 3.30–5.36 Ma); only magnetostratigraphically calibrated part younger than 7.3 Ma included for 907 (Channell et al., 1999). (B) Benthic (BE) and planktic (PL) $\delta^{18}O$ and $\delta^{13}C$ records from the N. Atlantic (ODP-982; Hodell et al., 2001; re-calibrations: Lawrence et al. (2009), Drury et al. (2017)), S. Atlantic (1085; Westerhold et al., 2005), N. Adriatic Sea (Monte del Casino; Kouwenhoven and van der Zwaan, 2006), Mediterranean (Pliocene stack; Wang et al., 2010), and global oceans (Pliocene stack; Lisiecki and Raymo, 2005). (C) precipitation levels estimated from micromammals (this paper) for localities with age uncertainty ≤200 kyr; squares: average monthly level, left triangle: driest month level, right triangle: wettest month level, blue arrows: trends, black: Teruel Basin, green: Bajo Segura Basin, red: Granada Basin, magenta: Cabriel and Júcar Basins, pink: Alcoy Basin, yellow: Guadix-Baza Basin. (D) Eccentricity record (Laskar et al., 2004); astrochronozone numbering after Hilgen et al. (2020); black line: eccentricity, grey line: envelope (100-kyr maxima). (E) proportion (semi-)aquatic species in non-aerial micromammal community (f(aq)), and major sedimentary units in Teruel Basin (Mein et al., 1990; Opdyke et al., 1997; Alcalá et al., 2000; van Dam et al., 2001; this paper); Units I-V according to Alcalá et al. (2000), blue arrows: trends f(aq), blue bars: lacustrine/palustrine facies. (F) Obliquity record (Laskar et al., 2004); astrochronozone numbering after Hilgen et al. (2020). (For interpretation of the references to colour in this figure legend, the reader is referred to the web version of this article.)

event was correlated to a (low-resolution) isotopic event as observed in northern Atlantic site ODP-608 (MTi4; Abreu and Anderson, 1998). With site ODP-1085 potentially affected by Antarctic Circumpolar (in addition to North Atlantic) Deep Water, this positive excursion may have been triggered by one of a series of major glaciation pulses on Antarctica. Cross-equatorial atmospheric forcing with northward ITCZ shifting would then have to be invoked as a mechanism for transporting the effects to the Northern Hemisphere (NH) (as similarly hypothesized for the Middle Miocene; e.g., John et al. (2003), Holbourn et al. (2010)). A peak in Southern Hemisphere (SH) glaciation may thus have led to a climatic perturbation in the northern part of the NH subtropical-dry region (for instance as a drying event at the Ib-N11-12a boundary, Section 4.2). Besides the hypothetical nature of this teleconnection, there is a small discrepancy in timing (7.67–7.66 Ma for the fauna, maximally 7.60 Ma for MTi4) that still needs to be explained.

No major well-known open ocean $\delta^{18}O$ events are associated with the Ib-N12a-b and 12b-13a transitions at ~7.15 and ~ 6.95 (Fig. 3B). As can be seen in Fig. 3B, it is not until 6.4 Ma that strongly positive values are recorded ('C3An.1n events', Fig. 3B). These events (which are preceded by a negative shift in $\delta^{18}O$ culminating at 6.43 Ma) herald the onset of the so-called 'Messinian glaciation'. Cooling is also observed in the Atlantic SST record at this time (Fig. 3A). Because of the large age uncertainty associated with the Ib-N13a-b boundary, it is not possible to establish whether faunal change is associated with this cooling or with the preceding warming.

The Ib-N13b-c boundary at 6.26–6.25 Ma correlates to the end of the 'C3An.1n-events' period and to low SST values between 6.37 and 6.24 Ma (e.g., C3An.18O.14/16 at 6.28 and 6.24 Ma; Hodell et al., 1994). The entry of the African rodent immigrant *Paraethomys* as recorded in sites Venta del Moro and Sifón de Librilla 52 (~6.25 Ma) may have occurred during the second of these isotopic events. If this was indeed the case, faunal change at the Ib-N13b-c boundary would qualify as an example of high-latitude forcing (via sea level). At the same time, this case is unique, as the Messinian is the only interval during which this type of direct immigration from Africa would have been possible. (We note that besides *Paraethomys* also other lineages such as *Myocricetodon* and *Debruijnimys almenarensis* crossed the Gibraltar barrier. However, because of their rarity and poorly constrained ages, their first appearance cannot be dated with accuracy and could even be coeval with that of *Paraethomys*.)

Perhaps surprisingly, both the onset of the Messinian Salinity Crisis (5.96 Ma) and the two well-known glacial events TG20/22 and TG12 (5.75–5.80 and 5.55 Ma; Shackleton et al., 1995; Fig. 3B) are not associated with any zone boundary. Similarly, no major open ocean climatic event ($\delta^{18}O$ and/or SST) is recorded at the Ib-N13c-14a boundary (range 5.47–5.33 Ma). If any climatic link to the Ib-N13c-14a boundary had to be made, it would be the occurrence of the 'interglacial' interval at 5.5–5.3 Ma (Fig. 3A,B).

The Ib-N14a-b boundary (4.91–4.87 Ma), which involves the disappearance of *Celadensia* and the simultaneous expansion of *Paraethomys* (two lineages) and *Stephanomys*, correlates to well-known glacial event Si6 at 4.89 Ma (Shackleton et al., 1995). The possibility cannot be excluded that also *Promimomys*, the first arvicoline immigrant in Europe, entered the Iberian Peninsula during Si4–6. However, in contrast with south-eastern Europe (where it is already well-represented from 5.3 Ma onwards; Hordijk and de Bruijn, 2009), *Promimomys* had a very marginal presence on the Iberian Peninsula with occurrences in only three not very accurately dated Ib-N14b faunas of the Teruel Basin (La Gloria 4, Celadas 9/12; Adrover et al., 1993; van Dam et al., 2023). The lack of any sign of SST cooling until 4.0 Ma west of Gibraltar (U1387, record starting 5.4 Ma; Tzanova and Herbert, 2015) may be due to low sampling resolution (Fig. 3A). In Greece and on Sicily, on the other hand, a drying effect of event Si6 has been inferred based on an expansion of herbs including *Artemisia* (Kloosterboer - van Hoeve Kloosterboer - van Hoeve, 2000).

Whereas the Ib-N14b-c and Ib-N14c-15a transitions (4.71–4.51,

4.27–4.19 Ma) are not associated with any well-known high-latitude climatic event (Fig. 3B), the Ib-N15a-b boundary (4.01–3.92 Ma) temporally correlates to glacial event Gi20 (4.00 Ma; Lisiecki and Raymo, 2005). On the other hand, the long Zone Ib-N15b (~4–3.2 Ma) bridges well-known glacial events such as Gi2/4 (3.67, 3.63 Ma) and M2 (3.30 Ma).

The lack of a clear expression of the global $\delta^{18}O$ event M2 at 3.3 Ma not only characterizes the Spanish rodent record, but also the Mediterranean SST record (Fig. 3A). Likewise, the astronomically calibrated record of Punta Piccola (Sicily, representing the 3.7–2.6 Ma part of the Mediterranean composite SST record of Herbert et al., 2016; Fig. 3A) is not showing any glacial peak at this time. Similarly, the ensuing Ib-N15b-16a transition at 3.19–3.18 Ma and the Ib-N16a-b transition at 3.06–3.03 Ma do not correspond to any well-known glacial event. The apparent 'immunity' of Mediterranean terrestrial environments to these events seems to contrast with biotic responses in more northern areas; for instance, pollen records from Norway show an expansion of (similar to present-day) alpine 'cool' vegetation around 4.2–4.0 and 3.4–3.3 Ma (Panitz et al., 2016), intervals that include well-known cooling events Gi20 and M2, respectively.

The Ib-N16b-17a boundary at 2.56–2.54 Ma is temporally very close, although slightly preceding isotope stage MIS 100 (2.52 Ma). Together, stage 100 and stages 98 and 96 at 2.49 and 2.43 Ma represent the first important glacial phase of the Early Pleistocene (e.g., Lisiecki and Raymo, 2005; Fig. 3B). At 2.52–2.51 and 2.48 Ma, Mediterranean SST drops ~5 °C and Atlantic SST decreases as well (ODP-982, Fig. 3A). The next rodent boundary (Ib-N17a-b at 2.15–2.05 Ma) also coincides with the onset of a series of strongly ^{18}O-enriched peaks (stage MIS 78 at 2.12 Ma, followed by stage 82 at 2.07 Ma), and with another Mediterranean SST drop (2.08–2.06 Ma). The top of Ib-N17b (1.9–1.8 Ma), on the other hand, is not associated with a single specific, well-known $\delta^{18}O$ event.

In summary, the evidence for a triggering of Iberian faunal transitions by high-latitude climatic/glaciation events is relatively thin for the latest Miocene and Pliocene (8.7–3 Ma, exceptions being events Si4–6 at 4.9 Ma and Gi-20 at 4.0 Ma), but relatively strong for the earliest Pleistocene (2.5–2 Ma).

4.2. Regional events

In this section we compare the timing of Iberian rodent transitions to regional, Mediterranean-wide marine proxy records (SST, planktic $\delta^{13}C$ and $\delta^{18}O$) as well as to our own Iberian paleoprecipitation and lake expansion/contraction records. Several important tectonics-related observations will be included into this discussion as well.

4.2.1. Late Miocene climatic and tectonic events

Because both North Atlantic and Mediterranean SST records fail to show any clear sign of cooling around 7.6 Ma (Fig. 3A,B) other explanations for rodent turnover should be explored. Here, we favor a link of Iberian records to the sudden 1.5–2‰ negative shift in surface water $\delta^{13}C$ starting at 7.63 Ma and culminating at 7.60–7.58 Ma, as reported for northern Italy (Monte del Casino section; Romagnan Appenines; Kouwenhoven et al., 1999). According to Kouwenhoven and van der Zwaan (2006) this shift could well be related to increased runoff from the continental (and hence ^{13}C- depleted) hinterland (sensu Gudjonsson and van der Zwaan, 1985), in turn attributed to the emergence of Italian and Alpine landmasses. The planktic $\delta^{18}O$ record from Monte Casino shows a shift towards more depleted values at 7.6 Ma as well, which, given the lack of any major global SST change at that time, can best be interpreted as an increase of the contribution of fresh water (e.g., Rohling, 1999). An overall increase of precipitation and runoff in northern Italy coincides with an increase of precipitation in the Teruel Basin, as evidenced by the transition from a drier Ib-N11 Zone (average MAP of 475 mm; driest month with zero precipitation) to an overall wetter Ib-N12a Zone (average MAP of 633 mm, driest month with non-zero precipitation in ~60% of the sites; Table S3, Fig. 3C; similar results were attained by van Dam (2006)). The increase in precipitation around 7.6 Ma is consistently associated with an increase of the average proportion of (semi-)aquatic micromammals from 0.01 in Ib-N11 to 0.08 in Ib-N12a.

Precipitation increase at the transition from Ib-N11 to N12a is consistent with lake expansion in the Teruel Basin as indicated by an increase in carbonate/marl lithologies (Fig. 3E). In fact, the age of the boundary (7.68–7.65 Ma) exactly coincides with a major lithological switch from alluvial to lacustrine sediments as recently dated for the base of a 30 m thick cyclic, limestone/marl unit in the Concud area (van Dam et al., 2023). This unit correlates to various other local carbonate-dominated bodies in the basin that have collectively been informally named 'Páramo 1' (e.g., Godoy et al., 1983; Unit II of Alcalá et al., 2000; genetic unit TN3 of Ezquerro et al., 2020; Fig. 3E). For instance, 3–4 km north and northeast of Concud this unit is 15-20 m thick and likewise associated with N12a/b sites (Las Casiones and Lomas de Casares sections: localities la Casiones 2 and Barranco de Cuevas 1–4; Mein et al., 1990; van Dam et al., 2001). Lacustrine sedimentation started somewhat earlier in the more central and central-eastern parts of the basin (Fig. 3E), where carbonate/marl series are recorded just above the Ib-N11 sites Masada Ruea 2 (8.5 Ma), Los Aguanaces 1/3, Alfambra (8.3 Ma), Tortajada A (8.2 Ma) and El Búnker 6/7 (= Valdecebro 4, 7.9 Ma) (van Dam et al., 2001). Precession cycle counting in the Concud area has yielded an age uncertainty range of 7.05–7.00 Ma for the top of the Páramo 1 unit. Whether this top is isochronous across the basin is unsure; for instance, in the El Búnker section its age uncertainty interval is estimated at 7.00–6.71 Ma (van Dam et al., 2023).

The observed correspondence between precipitation increase and lake expansion suggests an important role for climate in addition to tectonic subsidence as an agent for lake formation in the Teruel basin. In the Bajo Segura Basin, a MAP increase is observed as well, with mean values increasing from 388 to 574 mm between Ib-N11 and N12a ($n = 4$ and 2 sites, respectively). The return of the hamster *Cricetulodon* in this basin in Ib-N12a (Freudenthal et al., 1998) is consistent with a humidity increase, as can be inferred from its earlier disappearance from the Iberian record at 9.5 Ma during a drying episode associated with the 'Vallesian Crisis' (van Dam, 2006; Casanovas-Vilar and Agustí, 2007). Finally, the large mammal record is consistent with the small mammal record in showing wetter conditions in Ib-N12a-correlative sites as revealed by the analysis of microwear and diet in ruminants (Teruel Basin; De Miguel et al., 2019).

The recent study of time-equivalent sediments in the Jumilla-La Celia basin in the northeastern Betics (~7.6–6.9 Ma; van Dam et al., 2014; van Balen et al., 2015; van Dam et al., 2023; Fig. 1) has shown that large-scale lacustrine conditions did not develop, but that small lakes were present at 7.6–7.5 Ma and 7.3–7.2 Ma as evidenced by the presence of carbonate and gypsum deposits (Los Barracones section). A parallel section (La Celia section) consists almost entirely of siliciclastics, but the excess production of paleosol carbonate reveals at these same times reveals the occurrence of wetter conditions also there. A specific dry event as recorded in the in the Bajo Segura Basin around 7.65 Ma has thus far not been encountered, but future study may reveal its existence.

At ~7.65 Ma, the composition of the Ib-N11-12a transitional fauna Crevillente 4 in the Bajo Segura Basin differs markedly from typical Ib-N11 as well as Ib-N12a compositions by peak occurrences of *Apocricetus* and the *Parapodemus gaudryi* - *Apodemus gudrunae* lineage well before these forms become regular inhabitants (in Ib-N13b). A low diversity for CR4 (only six terrestrial rodents and one eulipotyphlan) points to arid conditions, which is confirmed by a predicted mean MAP of only 220 mm/yr (Table S3). Consistently, *A. mystacinus*, the supposed living descendant of the latter lineage (Martín Suárez and Mein, 1998) is currently restricted to the drier region of southwestern Europe and the Middle East. Finally, the unique late presence of crocodiles at this site (Böhme and Ilg, 2003) further indicates special conditions with temperatures being higher than before or after this time.

Interestingly, the Ib-N11-12a boundary overlaps with the 'Tortonian

Salinity' crisis, a short interval of evaporite deposition in the eastern Betics in SE Spain, which has been dated at 7.8–7.6 Ma (Krijgsman et al., 1999). Although no indications for a specific drying event can be inferred from the sea surface isotopic records of the Adriatic Sea (which only indicate the shift to wetter conditions, Fig. 3B), there is recent age information for a significant drying event ('Khersonian drying') between 8.02 and 7.84 Ma in the Paratethys domain that ends at 7.65 Ma ('Maeotian transgression'; Palcu et al., 2019, 2021; Butiseaca et al., 2021) time-correlative with the Ib-N11-12a boundary. Possibly this drying event was not even restricted to Europe, as suggested by the documentation of a late Miocene low in (wet season) precipitation in China at 7.6 Ma as well (Hui et al., 2023). Whether Eurasian drying was leading in bringing aridity to the peripheral Iberian Peninsula, or all areas responded to a single external, even more remote event (e.g., Antarctic glaciation, Section 4.1) cannot be established with certainty. In any case, a tectonic explanation for evaporite deposition in southern Spain (uplift leading to the formation of a submarine sill and partial isolation of marginal basins in the Eastern Betics; Krijgsman et al., 1999) could be supplemented by a climatic explanation.

After a long period of stable and high SST levels of ~27–28 °C or higher between 9 and 7.5 Ma, a surprisingly low SST in the Mediterranean Sea (Adriatic region) is recorded between 7.5 and 6.6 Ma (Tzanova et al., 2015). During two successive peaks, SST dramatically drops to ~20 °C, i.e., even lower than at North Atlantic site ODP-982. (A comparable SST drop has recently been recorded in the eastern Mediterranean; Kontakiotis et al., 2022). The first cooling peak starts at 7.28 Ma and then culminates at 7.19 and 7.14 Ma. After a short reversal, SST drops again with strong minima at 6.92 and 6.85–6.84 Ma. Both cooling phases would qualify as potential triggers for faunal change, with the first event corresponding to the Iberian Ib-N12a-b boundary (between 7.18 and 7.09 Ma), and the second event falling in the uncertainty range of the Ib-N12b-13a boundary (7.02–6.90 Ma). Alternatively, the latter transition could correspond to the preceding SST rebound to 27.0 °C at 6.97 Ma, or to a combination of the two events.

The nature of the two Mediterranean cooling peaks centered at 7.2 and 6.9 Ma is rather enigmatic, as a clear expression in open ocean records is lacking and both events precede the SST drops in the open ocean associated with the major phase of the 'Messinian glaciation' starting at 6.3 Ma (Fig. 3A). A small SST drop is recorded at ODP-982 at 7.2 Ma, but not at 6.9 Ma, whereas the ODP-907 record shows no sign for strong cooling events at all. A moderately strong, positive step in the $\delta^{18}O$ record in ODP-982 occurs at 7.14–7.135 Ma (Fig. 3B), but at this time Mediterranean SST starts to rise again. The relatively low resolution of the samples used for SST reconstruction (especially for site 982) may play a role, however.

The occurrence of a strong regional cooling during the early Messinian is consistent with the 'siphon event' hypothesis (Hodell et al., 1989; Benson et al., 1991) involving a current reversal event through the Rifian Corridor by which cool waters from below the Atlantic thermocline are injected into the Mediterranean. The planktic record of the Adriatic Sea may reflect this event (Kouwenhoven et al., 1999) with various strong positive $\delta^{18}O$ spikes at 7.14 Ma, and at 6.97, 6.94 and 6.85 Ma correlating to the above-mentioned cooling events. The simultaneous occurrence of positive $\delta^{13}C$ excursions in the Adriatic record (Fig. 3B) seems more difficult to explain, however, because the influx of below-thermocline Atlantic source waters is expected to lead to more negative $\delta^{13}C$ values. Here we suggest that stronger, SST-dependent carbon isotopic equilibrium fractionation effects during air-sea CO_2 exchange played an important role (~0.1‰/°C, Zhang et al., 1995) with potentially strongly counteracting non-equilibrium effects (e.g., see Schmittner et al., 2013) being subdued in the restricted Mediterranean setting. With significant productivity increase being ruled out (Kouwenhoven et al., 1999) the only other explanation for these $\delta^{13}C$ maxima would be a temporary reduction of continental runoff. However, such a reduction is not expected in an otherwise active tectonic regime (van der Meulen et al., 1999).

With the final disappearance of *Huerzelerimys* and *Cricetulodon* at the Ib-N12a-b transition (7.18–7.09 Ma), Iberian faunal structure starts to echo that of Ib-N11, as evidenced by a low faunal diversity, the re-expansion of *Occitanomys* and the re-occurrence of *Parapodemus lugdunensis* (in the Teruel Basin, van Dam et al., 2023). The resemblance of Zone Ib-N12b to N11 is consistent with the very rapid return to higher Mediterranean SST temperatures of 24–25 °C at the base of Ib-N12b (7.13 Ma, and to a lesser degree also at 7.18 and 7.09 Ma, Fig. 3A). On the other hand, it should be noted that drying is observed to start already high in Ib-N12a (~7.25 Ma) as indicated by the disappearance in the Teruel Basin (Tortajada, Concud Cerro de la Garita 5, Aljezar B) of aquatically adapted and arboreal species (with the latter loss translating into zero precipitation in the driest-month, Fig. 3C). These seasonally dry conditions, which normally apply to the summer in western parts of continents (including the Mediterranean region; Henderson-Sellers and Robinson, 1994; Bosmans et al., 2015a), basically persist throughout the remaining part of the Miocene (van Dam, 2006). On the other hand, the continuing presence of invertivorous groups indicates reasonably high precipitation levels during the rest of the year, as reflected in mean MAP values exceeding 500 mm in these higher placed Ib-N12a sites (Table S3), and also in Zone Ib-N12b (La Roma 5A, Valdecebro 5), where values of 600 mm are occasionally reached (not in Table S3, because age uncertainty >200 kyr).

A low level of faunal similarity between Iberian Basins during Ib-N12b and across the Ib-N12a-b transition (van Dam et al., 2023) points to the existence of important barriers, for which mountain ranges constitute the best candidates. The idea of enhanced tectonic activity leading to topographic barriers at this time is supported by several lines of evidence, including the intensification of volcanic activity in south-eastern part of the Iberian Peninsula at ~7.7 Ma (Fortuna Basin; Kuiper et al., 2006) with a marine to continental transition occurring at 7.6 Ma (Garcés et al., 2001). Volcanic rocks in association with diapirism of Triassic gypsum in the Jumilla-La Celia Basin (Fig. 1) have been radiometrically dated at ~7.6–7.2 Ma (Nobel et al., 1981; van Balen et al., 2015) and magnetostratigraphically dated at 7.6–7.5 (tuffaceous marl and basalt) and 7.05 Ma (ash and clasts) (van Dam et al., 2023). It may not be coincidental that a major phase of diapirism of Triassic evaporites is recorded in the Teruel Basin as well around this time (Tortajada Formation, van de Weerd, 1976; Alonso-Zarza and Calvo, 2000). Specifically, we report a transition from limestone to gypsum occurring a few meters above the Ib-N12a site Tortajada Pueblo (van Dam et al., 2023). Also, other local gypsum bodies in the basin are associated with Ib-N12a sites, for example at Los Mansuetos (Calvo et al., 1999) and Los Aljezares (see: López-Martínez, 1989). Somewhat higher in the sequence (locality Modorras, Zone Ib-N13b or N13c) gypsum and alluvial beds interfinger. The age of the top of the Tortajada Formation is poorly constrained but appears to project at least into Zone Ib-N13b (above sites Masada del Valle 7 and Regajo 5; van Dam et al., 2001), for which a maximum age of 6.56 Ma was inferred (Table 1). From the viewpoint of general basin formation, however, there are no major indications for a major tectonic pulse in the Teruel Basin around this time, with Zone Ib-N12a positioned in the middle of a major tectonic unit (TN3, Ezquerro et al., 2020) and relief rejuvenation and alluvial fan development occurring ~1 Myr later (TN3–4 transition). In a broader context, however, the ~7.6–6.8Ma interval corresponds to a period of increased tectonic activity in the Mediterranean (leading up to the Messinian Salinity Crisis; Krijgsman et al., 1999, 2018) and Alps (Valla et al., 2012).

Contemporary with a short period of fluctuating Mediterranean SST (Fig. 3A), the Iberian fauna was truly reshuffled at the Ib-N12b-N13a transition (between 7.02 and 6.90 Ma). New lineages (*Stephanomys* and a second, small-sized *Occitanomys*) enter, existing lineages re-expand (*Parapodemus gaudryi* - *Apodemus*, *Neocricetodon*) or rapidly transform (*P. barbarae* - *Castromys*). At this point it is worthwhile to note that the improved stratigraphic resolution for the 7.4–6.8 interval (van Dam et al., 2023) now shows that faunal changes previously considered

to belong to one event (SM13 event of van Dam (1997), MME 1 event of Agustí et al. (2006)) are distributed across two phases that correspond to zone boundaries Ib-N12a-b and N12b-13a.

The only well-documented fauna in the Teruel Basin just after the Ib-12b-13a transition (Gloria 6, Ib-N13a) has an associated estimated mean MAP of ~500 mm, i.e., comparable to the preceding upper Ib-N12a and N12b faunas. The fauna nevertheless witnesses the return of the arboreally-adapted dormouse *Muscardinus*, pointing to a temporary increase in summer precipitation. By contrast, the Ib-N13a fauna Crevillente 22 (age between 6.78 and 6.60 Ma) in the Bajo Segura Basin has an estimated mean MAP of only 350 mm, which is lower than that of Ib-N12b faunas in that area. As already mentioned in Section 3.2, estimates for the more eastern Fortuna Basin (Sifón de Librilla) are extremely low reflecting the almost complete absence of insectivorous species. Possibly these low levels could be linked to two strong, concerted positive $\delta^{13}C$ and $\delta^{18}O$ excursions at 6.7–6.6 Ma (still within Ib-N13a, Fig. 3A) as recorded in Adriatic surface waters (Kouwenhoven and van der Zwaan, 2006; Fig. 3A) indicating a reduction of freshwater runoff (aridity).

With an average MAP of ~400 mm/yr, Ib-N13b faunas from the Teruel Basin are associated with somewhat drier conditions than Ib-N12b-13a faunas (sites not shown in Fig. 3C, because of large age uncertainties, but see van Dam (2006)). Consistently, Ib-N13b witnesses the expansion of the *Parapodemus gaudryi - Apodemus gudrunae* lineage that also peaked at the dry Ib-N11-12a 'boundary event' (Section 3.2). The entry in Ib-N13b of *Blancomys*, a hamster with robust, hypsodont molars, is also consistent with drying. Although the Mediterranean SST record shows high values until 6.4 Ma (start of a gap in this record, Fig. 3A), the association of Ib-N13b to warm sea water conditions cannot be demonstrated unequivocally, because of the large age uncertainty surrounding the Ib-N13a-b boundary (6.56–6.27 Ma, Table 1).

MAP values are very low for the Granada Basin around the Ib-N13b-c transition (Fig. 3C), which would be consistent with the expansion of the terrestrial, supposedly dry-adapted African rodent immigrant *Paraethomys* at this time (6.24–6.23 Ma, MME 2 event of Agustí et al., 2006). Values for the more eastern Fortuna Basin are even drier (Sifón de Librilla).

4.2.2. Pliocene and early Pleistocene climatic events

The Ib-N13c-14a boundary (between 5.47 and 5.33 Ma) correlates to the final phase of the Messinian Salinity Crisis between 5.55 and 5.33 Ma (Upper Gypsum/Lago Mare; Krijgsman et al., 2018). Differences between 'Late Miocene' Ib-N13c and 'Early Pliocene' Ib-N14a faunas in the southeastern basins (Alcoy, Fortuna, Granada Basins) are surprisingly small, however (Fig. 2A), which seems at odds with the extreme paleogeographic changes that would accompany a (partly) desiccated Mediterranean. More to the north (Teruel Basin), on the other hand, faunal change between Ib-N13c and 14a is more marked because of the immigration of *Celadensia*, the first 'vole-like hamster' to enter the Iberian Peninsula. *Celadensia* has more hypsodont and prismatic molars compared to typical hamsters, which can be seen as an adaptation to a more herbivorous diet and to the contamination by grit and soil associated with more open landscapes (Jardine et al., 2012). (This type of dental morphological change foreshadows a trend that is further perfected in arvicolines, see below.) *Celadensia* is morphologically similar to the eastern genus *Microtodon* as initially defined on material from Inner Mongolia (Fejfar et al., 2011). Its subsequent entry in Greece is dated at 5.40–5.23 Ma (Hordijk and de Bruijn, 2009), an interval that overlaps with the uncertainty range surrounding the entry of *Celadensia* in Spain. As this entry occurs during the period of Mediterranean desiccation (5.59–5.33 Ma, Krijgsman et al., 1999) dispersal to the Iberian Peninsula may have been eased by the creation of new migration routes.

Given its Asian affinities, we hypothesize that a preadaptation to continental (cooler, more seasonal) conditions allowed *Celadensia* to preferentially colonize the northern, interior and higher-altitude parts of our study area (Teruel Basin). Precipitation values in this area during Ib-N14a show a small rise, which agrees with the temporary expansion of waterbodies (Fig. 3E). Zone Ib-N14a faunas in the Teruel Basin also witness the re-appearance of the jumping mouse *Eozapus* (Dipodidae), a form well represented in Central Europe (with occurrences at latitudes as least as high as the level of Poland), and the temporary presence of a lineage of the murine *Micromys*, a form especially well represented in the eastern Mediterranean (Greece, Turkey; Hordijk and de Bruijn, 2009). Although these latter two genera are rare in Spain (they belong to one of our rest groups), their entry together with that of *Celadensia* in the central region can be regarded as the start of an important series of Plio-Pleistocene Central-Eastern European rodent invasions into the Iberian Peninsula. (The entry of the rare hypsodont hamster *Blancomys sanzi* at the Late Miocene Ib-N13a-b transition in Central Spain may be regarded as an early precursor of these events.)

The Ib-N14a-b, N14b-c and N14c-15a transitions around ~4.9, 4.6 and 4.2 Ma are not associated with distinct changes in SST at Mediterranean latitudes (including the Gulf of Cadiz, Fig. 3A). However, especially the latter two transitions are associated with low values in both Mediterranean planktic $\delta^{13}C$ and $\delta^{18}O$ (Wang et al., 2010; Fig. 3B). Freshwater input is the most widely accepted process to explain these intervals with low $\delta^{13}C$ (Gudjonsson and van der Zwaan, 1985) and $\delta^{18}O$ (Lourens et al., 1992). These intervals are also associated with an increased deposition of organic-rich beds (equivalent to younger sapropels) of which the genesis is explained by an increase in circum-Mediterranean humidity (Rossignol-Strick, 1985). Consistently, the successive colonizations of the Iberian Peninsula by the vole-like hamster *Trilophomys* and the true vole *Mimomys davakosi* at the Ib-N14b-c and N14c-15a boundaries fit a humidity-related scenario, as both forms are common at more northern latitudes in both Western and Eastern Europe where precipitation levels are higher (van Dam, 2006; van Dam and Utescher, 2016). Consistent with the absence of a clear correlation to Mediterranean $\delta^{13}C$ and $\delta^{18}O$ (Fig. 3B) and a pollen-based indication for aridity during glacial event Si6 (4.89 Ma, Section 4.1), a second, larger-sized Iberian lineage of the African-derived potentially dry-adapted genus *Paraethomys* appears and expands at the Ib-N14a-b transition (4.91–4.87 Ma). Very low (Fuente del Viso) or moderately low (Alcoi 0) precipitation levels as predicted for eastern Spain during Ib-N14b (Fig. 3C) are consistent with these observations.

An average MAP of ~330 mm (range: 200–600 mm) characterizes the well-dated and well-covered upper Ib-N14c to lower N15b interval in the Teruel Basin. Two estimates for the southern Guadix-Baza Basin (Gorafe 1 in Ib-N14c and Gorafe 2 in Ib-N15b) reveal very low values of 100-200 mm. The entry of the flying squirrel *Pliopetaurista* in Ib-N15a (Villalba Alta Rio 2, 4.16 Ma) indicates the start of period of increasing tree density and non-zero precipitation during the driest month (Fig. 3C). On the other hand, winter rainfall decreases implying a reduction in rainfall seasonality. Whereas most of the Ib-N15a localities still lack *Pliopetaurista*, its presence becomes more permanent after 4.1 Ma (Ib-N15b). A more homogeneous rainfall regime appears to characterize the Iberian Peninsula as a whole; for instance, the Ib-N16a fauna Tollo de Chiclana 1B in the Guadix-Baza Basin (which also contains *Pliopetaurista*) has a comparable precipitation level as the more northern sites in the Teruel Basin.

A new phase of lake expansion in the Teruel Basin that is especially well recorded at Orrios (Fig. 3E) starts at ~4.5 Ma and lasts until ~3 Ma. Based on the more peripherally located sedimentary sequences at Villalba Alta Río and Escorihuela, we infer that lake area was maximal at 4.27–4.01 Ma (during Ib-N15a), between 3.57 and 3.46 Ma (an interval within Ib-N15b, but without localities) and ~ 3.3–3.0 Ma (during Ib-N16a), which is in line with the results of recent studies near Orrios and Villalba Alta (Ezquerro et al., 2022; Gao et al., 2022). The fact that the entry of the vole *Dolomys* coincides with lake contraction (at 4.0 Ma) seems at odds with its assumed semi-aquatic lifestyle. This latter assumption, which is based on Repenning et al. (1990) hypothesis of a relationship with the living muskrat *Ondatra* (tribe Ondatrini) has, in fact, been doubted by other workers (Martin, 2008). Moreover, locomotor styles are flexible in voles, as evidenced by the existence of a

Table 2
Iberian rodent zone boundaries with associated orbital configurations, hydrological changes, main murid dispersal events, glacial events and tectonically relevant events. Astrochronozone numbering after Hilgen et al. (2020).

Zone boundary	Age (Ma)		Obliquity amplitude	Eccentricity		Hydrology		Dispersal events	Correlations
	Maximum	Minimum	(1.2-Myr cycle)	(2.4-Myr cycle)	(405-kyr cycle)	(Precipitation)	(Teruel Basin lakes)	(New murid clades)	(Isotopic events, tectonics)
top Ib-N17b	1.90	1.80	min (3 → 2)	max (2)	max (5)			*Allophaiomys*	min. Med. surface $\delta^{13}C$-$\delta^{18}O$
Ib-N17a-b	2.15	2.05	min (3 → 2)?	min (2 → 1)	min (6 → 5)	similar/ uncertain			MIS 82,78
Ib-N16b-17a	2.56	2.54	max (3)	min (2 → 1)	max (7)	similar/ uncertain			MIS 100–96
Ib-N16a-b	3.06	3.03	min (4 → 3)	min (2 → 1)	max (8)	wetter→drier	contraction		min. Med. surface $\delta^{13}C$-$\delta^{18}O$
Ib-N15b-16a	3.19	3.18	min (4 → 3)	min (2 → 1)	max (8)	seasonality increase	expansion	*Mimomys hassiacus*	min. Med. surface $\delta^{13}C$-$\delta^{18}O$
Ib-N15a-b	4.01	3.92	min (5 → 4)	min (3 → 2)	min (11 → 10) / max (10)?	seasonality decrease	contraction	*Dolomys*	Gi20
Ib-N14c-15a	4.27	4.19	min (5 → 4)	min (3 → 2)	max (11)	drier→wetter	expansion	*Mimomys davakosi*	min. Med. surface $\delta^{13}C$-$\delta^{18}O$
Ib-N14b-c	4.71	4.51	intermediate	min (3 → 2)	max (12)	uncertain	expansion	*Trilophomys*	min. Med. surface $\delta^{13}C$-$\delta^{18}O$
Ib-N14a-b	4.91	4.87	max (5)	min (3 → 2)	min (13 → 12)	wetter→drier	contraction after expansion		Si4,6
Ib-N13c-14a	5.47	5.33	min (6 → 5)	max (3)	max (14) / min (14 → 13)?	drier→wetter		*Celadensia*	tectonics?→ Messinian salinity crisis
Ib-N13b-c	6.26	6.25	intermediate	max (3)	max (16)	drier?			tectonics / C3An18O.14,16 → Af.-Eur. landbridge
Ib-N13a-b	6.56	6.27	min (7 → 6)	max (3)	min (17 → 16) / max (16)?	wetter→drier	contraction		
Ib-N12b-13a	7.02	6.90	max (7)	min (4 → 3)	min (18 → 17)	similar/ uncertain	contraction		tectonics / regional SST anomalies
Ib-N12a-b	7.18	7.09	max (7)	min (4 → 3)	max (18)	wetter→drier	similar		tectonics / regional SST anomalies
Ib-N11-12a	7.68	7.65	min (8 → 7)	min (4 → 3)	min (20 → 19)	dry event, drier→wetter	expansion		MTi4, Paratethys drying and expansion

terrestrial to semi-aquatic spectrum within living species of *Arvicola* (Nowak, 1999; Chevret et al., 2020). Alternatively, *Dolomys* may have preferred small rivers rather than lake margins. Given the relatively low levels of wettest month precipitation during Zone Ib-N15b (Fig. 3C), lake reduction between 3.99 and 4.01 Ma could be related to the reduction of winter precipitation, with a certain base level of humidity still secured by (non-zero) summer precipitation.

Although more well-dated localities are needed to be certain, precipitation levels for Ib-N16b are relatively low. We note that a high percentage (44%) of (semi-)aquatic micromammals (two voles and two eulipotyphlans) in Ib-N16b fauna Concud Estación 1 (Fig. 3F) stems from a low richness of the total fauna, with estimated MAP amounting to 260 mm only. Precipitation for site Concud Estación 2 is somewhat higher (390 mm). The development of an aeolian dune field near Escorihuela between 2.9 and 2.6 Ma (Fig. 3E) suggests dry conditions (Rodríguez-López et al., 2012).

As noted in Section 4.1, the timing of the Ib-N16b-17a and N17a-17b boundaries (2.56–2.54, 2.15–2.05 Ma) corresponds to that of glacial events MIS 100 and 78, respectively. It is around 2.5 Ma but especially at 1.85 Ma, that the Mediterranean SST record finally shows a permanent drop after having stayed at a stable high level during the Pliocene, Fig. 3A). This cooling trend around the Plio-Pleistocene boundary compares well to trends as inferred from pollen (Garraf core, north-eastern Spain; Fauquette et al., 1998), although these appear to occur slightly earlier (2.9–2.7 Ma). Finally, our data for Ib-N17a and N17b faunas in eastern and southern Spain (Júcar and Guadix-Baza Basins) show a continuation of dry conditions without any significant summer precipitation. Like most Pliocene zone transitions, also the Ib-N16b-17a and N17a-17b transitions are associated with low values of Mediterranean $\delta^{13}C$ and $\delta^{18}O$ (Fig. 3B), suggesting temporary higher humidity levels. A small raise of MAP around the Ib-N16b-17a boundary in the Teruel Basin may also reflect this increase (Fig. 3D).

4.3. Orbital cycles

Although many of the climatic events described above find their ultimate origin in astronomical variations, orbital extremes do not always lead to proportionally strong climatic extremes (Zachos et al., 2001a). Because more subtle but persistent orbitally forced changes in local insolation patterns, precipitation (including seasonality) and vegetation are expected to affect rodent communities via ecological-scale processes (e.g., reproduction, survival and competition), a direct comparison between rodent transitions and astronomical curves may reveal additional insights into relevant forcing mechanisms.

Given the 10^{5-6} year-scale of biozones, our focus is not directed at individual ~21-kyr precession and 41-kyr obliquity cycles, but on longer-scale cycles of eccentricity and obliquity. It should be noted, however, that short-period cycles may affect proxy results based on fossil content, such as our precipitation proxies. This bias may take the form of aliasing: because mammal sites are bound to certain lithologies within small-scale cycles (usually organic-rich marl beds deposited near aquatic margins), reconstructions for (sets of) sites may be biased towards either drier (shallow facies) or wetter conditions (deeper facies). On the other hand, the relatively fixed structure of assemblages as observed across entire biozones suggests that this type of bias may not be extreme.

4.3.1. The overall pattern

The average duration of rodent zones Ib-N11-17b is 0.46 Myr. Looking more closely (Fig. 3), a clustering of zones into three 1.4–1.5 Myr intervals (7.6–6.2, 5.4–4.0 and 3.2–1.9 Ma) can be discerned (Fig. 3D, F). These compound intervals are separated from each other by long intervals of ~0.8–0.9 Myr corresponding to a single zone only (Ib-N13c and N15b, at 6.3–5.4, and 4.0–3.2 Ma, respectively). The oldest zone (Ib-N11) has a long duration as well (1.1 Myr). Excluding the three long zones, average zone duration reduces to 0.35 Myr. Given the previously established correlation of the long 2.4 Myr eccentricity cycle to Neogene rodent turnover (van Dam et al., 2006), an effect of the next shorter eccentricity cycle (405 kyr) is to be expected. The 460 and 350 kyr durations as calculated for average zone duration (including and excluding long zones) strongly suggest an imprint of this cycle on the timing of the rodent zones.

Whereas the three long zones Ib-N11, N13c and N15b are associated with strongly fluctuating eccentricity (middle parts of 2.4-Myr cycles 2–4, Fig. 3D; cycle numbers after Hilgen et al., 2020), the compound intervals are associated with intervals with low average eccentricity (2.4 Myr minima, Fig. 3D, Table 2). Several late Miocene zone boundaries associated with strong turnover, such as the Ib-N11-N12a boundary at 7.66–7.65 Ma and the Ib-12b-13a boundary between 7.02 and 6.90 Ma are additionally associated with low 405-kyr eccentricity values. (Although the uncertainty interval of the latter boundary includes a 100-kyr maximum at 6.96 Ma, it is associated with a minimum at the 400-kyr scale). An age of the Ib-N13a-b boundary close to that of the next 405-kyr eccentricity minimum at 6.5 Ma would fit this pattern, but the considerable age uncertainty for this boundary (6.56–6.27 Ma, Table 1) makes this correlation uncertain. During the Plio-Pleistocene, the 405-kyr eccentricity-biozone relationship appears to be largely reversed with most zone boundaries associated with maxima (at 5.4, 4.6, 4.2, 3.2, 3.0, 2.5, 1.8 Ma) and only two (at 4.9 and 2.1 Ma) to minima. (The correlation at 4.0 Ma is uncertain.)

Van Dam et al. (2006) noted a deviating Pliocene pattern of orbital forcing compared to the rest of the Neogene, with subdued rodent response and lake reduction instead of expansion during the 2.4-Myr eccentricity minima between ~4.9–4.4 Ma. Here, we suggest that this Pliocene 'reversal' in rodent turnover is due to a shift in the response to the 405-kyr cycle, with maxima not associated with central parts of 2.4-Myr minima turning into hydrologically critical intervals as well. As further discussed below, this phase reversal could best be explained by a slowly proceeding underlying change in the average global climate (late Cenozoic cooling) resulting in an equatorward migration of the temperate belt.

In addition to eccentricity, the distribution of biozone ages bears the imprint of obliquity. The long ~0.8 Myr zones are associated with a specific, low-amplitude expression of the 1.2-Myr obliquity cycle (cycles 6 and 4; Fig. 3F). The oldest zone (Ib-N11, 1.1 Myr duration), corresponds to such a low-amplitude obliquity cycle as well (cycle 8). (The relationship of these long zones with both long-period eccentricity and obliquity is not surprising, as these long cycles are astronomically linked; Laskar et al., 2004). As mentioned above (Section 4.1), zone boundaries and high-latitude glacial events are coeval twice during the Pliocene (Si6 at 4.9 and Gi20 at 4.0 Ma) and twice during the Early Pleistocene (MIS 100 at 2.5 and MIS 78, 82 at 2.1 Ma). During this latter interval NH ice sheets became permanent with obliquity becoming the dominant orbital parameter controlling ice volume and, in turn, global climate (Ruddiman et al., 1989; Lisiecki and Raymo, 2005). Pliocene events Si4–6 and Gi20 are associated with obliquity nodes, whereas MIS 100 is associated with a strong obliquity antinode. This latter configuration with obliquity varying maximally around 2.5 Ma (1.2-Myr cycle 3, Fig. 3F) figures in the hypothesis that especially strong 41-kyr obliquity minima associated with reduced summer insolation accelerate NH polar ice growth at this time (non-linear response; e.g., Lourens and Hilgen, 1997; see also Section 4.3.2). For earlier periods (late Miocene and Pliocene), on the other hand, a different type of more subtle obliquity forcing must be assumed, with the sustained absence of 41-kyr obliquity maxima during 1.2-Myr nodes playing a more important role. The approximate time equivalence of the 'Messinian glaciation' (6.3 to 5.5 Ma), our long zone Ib-N13c (6.25 to 5.5–5.3 Ma) and the lower-amplitude obliquity cycle between ~6.5–5.5 Ma (cycle 6, Fig. 3F) suggests obliquity forcing presumably via NH high-latitude climate. We will now proceed by discussing orbital relationships in more detail per epoch.

4.3.2. Late Miocene orbital forcing

According to classical theory (Milankovitch, 1930), the strongest expected correlations between Mediterranean climate and lower-frequency orbital parameters involve eccentricity (as a modulator of precession), because precession rather than obliquity is the dominant component in insolation at low- to middle latitudes. The temporal correspondence of the Ib-N11-12a boundary at 7.68–7.65 Ma with an extreme in the 405-kyr eccentricity cycle (minimum between cycles 20–19, Fig. 3D) thus fits the theory. On the other hand, an additional control of obliquity on Iberian hydrology could help to explain the occurrence of a dry event at this boundary (as recorded in the Bajo Segura Basin, Section 4.2.1) during the rare moment of overlap of a node in the 1.2-Myr obliquity cycle (~8.2–7.6 Ma) and minima in the 2.4-Myr eccentricity cycle (~7.7–7.2 Ma; Figs. 3D,F) and 405-kyr eccentricity cycle (centered at ~7.65 Ma). Although a remotely working high-latitude mechanism could have played a role as well at this moment (SH glaciation, Section 4.1.1), the persistence of weak 41-kyr obliquity maxima until ~7.6 Ma would be consistent with reduced regionally (Atlantic)-derived (winter) precipitation (see Bosmans et al., 2020). In any case, the response to the 405-kyr minimum at ~7.65 Ma (dry conditions as indicated by small mammals) differs from the one during the subsequent 405-kyr maximum (cycle 19), as well as that of the next minimum at ~7.25 Ma (both with relatively wet conditions; Fig. 3D, E). It is thus conceivable that stronger obliquity variation between 7.5 and 7.0 Ma (cycle 6, Fig. 3F) is preventing average conditions from becoming too dry in this interval.

The observed increase in humidity between 7.5 and 7.0 Ma cannot be linked to the eccentricity record in a simple and straightforward way. The suppression of the ~100-kyr cycle by the 2.4-Myr eccentricity cycle in this interval leaves the 405-kyr cycle as the only eccentricity cycle with a clear expression (cycle 19, Fig. 3D). From the viewpoint of insolation, the 'damping' of precession-related climatic extremes under low eccentricity leads to the prolonged absence of both extreme warm NH summers and cool NH winters (during high-seasonality precession minima) alternating with the absence of cool NH summers and warm NH winters (during low-seasonality precession maxima). The prediction of such 'intermediate' conditions seems inconsistent with the observed increase in precipitation and lake area during in the Teruel Basin this interval (Section 4.2.1, Fig. 3D).

The emergence of a distinct climatic signal during an interval that is otherwise orbitally 'balanced' implies the occurrence of non-linearities in the interaction between climatic and/or biotic/sedimentary components. A well-known high-latitude example of non-linear climate-related response is the increase of polar ice volume at long-period orbital nodes, which depends on the reduction of summer melting rather than winter growth during strong ~21-kyr precession minima (NH) or maxima (SH) or ~ 41-kyr obliquity maxima (Zachos et al., 2001b; Lourens and Hilgen, 1997). Other examples include lake expansion associated with 2.4-Myr eccentricity minima or maxima (van Dam et al., 2006), minima (Abels et al., 2009, 2010), maxima (Valero et al., 2014) and peatland expansion during 2.4-Myr minima (Valero et al., 2016).

Model results with near-modern boundary conditions (for temperature, CO_2, topography, etc.) predict net more humid conditions during eccentricity maxima associated with strongly expressed precession minima (NH), with positive effects on both Mediterranean summer and winter precipitation (Kutzbach et al., 2014; Bosmans et al., 2015a). The observed precipitation increase and lake expansion during low-

eccentricity interval Ib-N12a (Fig. 3D) seems at odds with these results. Here, we propose that it is the average global climate at the time of study (during coolhouse - icehouse climatic evolution; Westerhold et al., 2020) that controls the amplitude and phase of sedimentary and hydrological responses to long-term orbital cycles. Before ~7 Ma global temperatures were still between 5 and 10 °C higher on the Iberian Peninsula (van Dam and Reichart, 2009; Herbert et al., 2016), which was positioned well into the drier subtropical belt (average MAP in the studied Iberian Basins rises from ~450 mm in Ib-N11 to ~600 mm in Ib-N12a; driest-month precipitation increase from zero to non-zero values; Fig. 3D) south of a much wetter (warm temperate) central Europe (van Dam, 2006). With temperatures in Spain and western Europe remaining high until ~7 Ma, a decrease in summer evaporation during weakly expressed precession minima would help in explaining the existence of a more positive water budget. In addition to this potential decrease in evaporation, driest-month precipitation (LMP) estimates increase (reflecting the expansion of the arboreally adapted *Csakvaromys* and to a lesser degree *Muscardinus*). The mismatch between our proxy results and model results based on near-modern boundary conditions results could imply that the latter need some modification in order to properly model much warmer intervals such as the Miocene and earlier periods (see also Herold et al., 2010).

An alternative orbital explanation for the observed wetter conditions between 7.6 and 7.2 Ma involves obliquity. With this interval corresponding to the middle part of the well-expressed 1.2 Myr obliquity cycle (cycle 7, ~7.9–6.7 Ma, Fig. 3F), strong obliquity maxima should then be held responsible for an increase of Mediterranean winter precipitation, in line with some recent studies (Bosmans et al., 2015a, 2015b). Because it can be assumed that winter rainfall is quantitatively more important than summer rainfall in filling groundwater reservoirs, a link between obliquity and long-term lake expansion/contraction may be hypothesized. (On shorter time scales, however, precession would still be the orbital parameter controlling shallow lake level variations; e.g., van Dam et al., 2023). An obliquity-dependent scenario would be consistent with the clear expression of the 1.2-Myr obliquity cycle in records from the Chinese loess plateau between 7.5 and 4.5 Ma (Qin et al., 2022: fig. 9), where a higher magnetic susceptibility is associated with wetter conditions during obliquity antinodes (see Gao et al., 2022, and reference therein). As further discussed below (Section 4.6), pacing by the 1.2-Myr cycle would then be temporally decoupled from forcing by regular 41-kyr cycles, which, before the Messinian glaciation (van der Laan et al., 2012), are mainly restricted to intervals of low eccentricity (2.4-Myr minima) in marine (e.g., Hilgen, 1991; Lourens et al., 1996) and terrestrial settings, including the Teruel Basin (Abdul Aziz et al., 2004; Abels et al., 2008).

The next zone boundary (Ib-N12a-b, 7.18–7.09 Ma) post-dates the preceding eccentricity minimum at 7.23 Ma by 0.05–0.14 Myr. Putting aside alternative, tectonics-related explanations (Section 4.2.1), the timing of the Ib-N12a-b boundary could thus theoretically be affected by the resumption of strong 100-kyr eccentricity cycles associated with decreasing humidity after a long interval of low eccentricity corresponding to the transition between 2.4-Myr cycles 4 and 3. (Obliquity variation is still large during Ib-N12b.)

As mentioned in Section 4.3.1, the Ib-N12b-N13a boundary (7.02–6.90 Ma) is again coeval with a 405-kyr minimum (between cycle 18 and 17, Fig. 3D). Except for a strong reduction of lake area around this time, no drying event based on fauna like the one at ~7.65 Ma could be found. A low chronological resolution of micromammal sites could play a role here. On the other hand, the weakly seasonal climate associated with the negative eccentricity 'spike' at 6.90 Ma could temporary have led to a relaxation of one or more ecological barriers between regions, allowing new lineages (*Stephanomys*, *Castromys*, *Occitanomys alcalai*) to take over dominance. The second (potentially unrelated) Mediterranean SST cooling as recorded by Tzanova et al. (2015) at 6.92 Ma (and later, at 6.85–6.84 Ma, Section 4.2.1) could have boosted the faunal instability generated by orbitally forced changes.

As discussed in Section 4.2.1, the age of the top of the 'Páramo 1' at Concud in the Teruel Basin (between 7.05 and 7.00 Ma; van Dam et al., 2023) post-dates the first strong 100-kyr eccentricity maximum at 7.16 Ma after the low-eccentricity interval 7.7–7.2 Ma by at least 110 kyr (Fig. 3F). A similar delay in timing of large-scale (formation-level) lithologies with respect to long-period eccentricity has been described for older parts of the basin (Cascante area), with a 400-kyr/2.4-Myr eccentricity minimum at 9.7 Ma leading the establishment of full lacustrine conditions by ~130 kyr (Abels et al., 2008). Comparable lags have been detected with respect to the two next older (middle Miocene) long-term eccentricity minima (Madrid Basin; Abels et al., 2010). In this latter case, lags in the timing of large-scale lithological changes with respect to orbital parameters have been explained by a 'memory effect' in such a way that groundwater reservoirs must first be filled before a lake can form (Abels et al., 2010). Likewise, it will take a considerable time for the lake to finally disappear (e.g., at 7.0 Ma) because reservoirs will still feed the lake long after the surface water budget has turned negative. On the other hand, if obliquity is believed to be the dominant parameter affecting lake area, there would be less need to invoke a 'memory effect'-type of explanation given the approximate match of the maxima in lake area and obliquity amplitude (Fig. 3F).

The broad age uncertainty interval of the next transition (Ib-N13a-b, 6.56–6.27 Ma) includes both a 405-kyr eccentricity minimum and maximum, making the correlation uncertain. The fifth transition (Ib-N13b-c) coincides with a 405-kyr eccentricity maximum (cycle 16) but differs from all other transitions by the existence of a unique migration route between Africa and Europe. The terminal Miocene Ib-N13c-14a boundary uncertainty interval (5.47–5.33 Ma) includes a 100-kyr eccentricity maximum at 5.43 Ma, but also extends into the first of three 405-kyr minima (between cycles 14–13, 13–12 and 12–11 in Fig. 3D) that accompany/fringe the 2.4-Myr minimum centered at 4.7 Ma. In this respect, the orbital configuration is reminiscent of the one at 7.65 Ma (Ib-N11-12a transition), which likewise is associated with a minimum in 1.2-Myr obliquity amplitude variation (transition from cycles 8 to 7 in Fig. 3F).

4.3.3. Pliocene orbital forcing

Compared to the late Miocene, the Pliocene shows a dominantly reversed phase relationship between Iberian rodent transitions and eccentricity, with zone boundaries at 4.6, 4.2, 3.2 and 3.0 Ma associated with high eccentricity. Three of these boundaries (at 4.6, 4.2 and 3.0 Ma) correlate to centers of 405-kyr eccentricity maxima (where the 100-kyr cycle has a maximum expression; cycles 12, 11 and 8; Fig. 3D), while one boundary (3.2 Ma) correlates to the second strongest 100-kyr maximum within 405-kyr maximum 8. (The other strong 100-kyr maximum correlates to the 3.0 Ma boundary.) A similar configuration could characterize the Ib-N15a-b boundary at 4.0–3.9 Ma (association with the 100-kyr maximum at 3.93 Ma), although in this case the boundary age uncertainty is too large to exclude an alternative correlation to the 100/405-kyr minimum at 3.99 Ma (Table 1). In contrast to the first four boundaries mentioned above, the Ib-N14a-b boundary at 4.9 Ma shows a late Miocene-type of association to a 405-kyr/2.4-Myr eccentricity minimum.

The Pliocene zone boundaries at 4.6, 4.2 and 3.0 Ma that correspond to 405-kyr eccentricity maxima 12, 11 and 8 also correlate to minima in both Mediterranean planktic $\delta^{13}C$ and $\delta^{18}O$, for which, in turn, significant coherences with the 405-kyr eccentricity cycle were demonstrated (Wang et al., 2010; Fig. 3B). The inference of wetter conditions during eccentricity maxima as inferred from the marine record (Section 4.2.2) fits the observation that rodent immigrants entering Spain during these transitions originate from more northern, temperate latitudes in both Western and Eastern Europe (*Trilophomys*, *Mimomys davakosi*, *M. hassiacus* and *Kislangia* at 4.6, 4.2, 3.2 and 3.0 Ma, respectively, and possibly *Dolomys* at 4.0 Ma, although the phase relationship with the 405-kyr cycle is uncertain; Fig. 3, Table 2). The association of these vole-like hamsters and voles with relatively humid conditions is supported by

a comparison of time-equivalent lacustrine and karstic localities in Spain (van de Weerd and Daams, 1978), showing that these groups abound in the former type of environments, while true mice have larger abundances in upland sites. The correspondence between 100-kyr and 405-kyr eccentricity maxima and higher Pliocene humidity is supported by recent work in the Teruel Basin on magnetic susceptibility variation (4–3.6 Ma; Gao et al., 2022) and carbonate oxygen isotope ratios (Ezquerro et al., 2022), respectively, although in the latter study temperature is expected to play a role as well. Finally, our interpretation of the climatic effects of the 405-kyr cycle during the Pliocene is consistent with marine and terrestrial cyclostratigraphic studies in the Gulf of Cadiz (Sierro et al., 2000) and Guadix-Baza Basin (Agustí et al., 2001) that indicate overall drier conditions in southern Spain during Pliocene 405-kyr minima.

The correlation of slightly enhanced precipitation rates and especially lake expansions in the Teruel Basin at 4.3–4.0 and 3.3–3.0 Ma (as indicated by distribution maxima of the 'Páramo 2' lithostratigraphic unit of Godoy et al., 1983; Unit IV of Alcalá et al., 2000; upper part TN4-lower part TN5 of Ezquerro et al., 2020; Fig. 3F) to periods of minimum obliquity amplitude variation (1.2-Myr cycle) once more suggests a control of obliquity on the regional water cycle (Fig. 3D,F). As in the case of eccentricity, the phase relationship with lake level is opposite to the ones before that time, when lacustrine facies complexes reached their maximum size during periods of maximum obliquity amplitude (between ~7.5–7.0 Ma (Fig. 3F) and between ~9.7–9.0 (van Dam et al., 2001; Abels et al., 2008)). The reversal in the expression of the 1.2-Myr obliquity cycle between the Miocene and Pliocene fits recent results from the Chinese loess plateau (Qin et al., 2022), where a typical late Miocene correlation between 1.2-Myr obliquity antinodes and wet conditions (as indicated by magnetic susceptibility) disappears around 4.5 Ma. The recovery of individual 41-kyr obliquity cycles in magnetic susceptibility between 3.3 and 3.18 Ma in the Teruel basin (Gao et al., 2022) fits observations of a globally increasing influence of obliquity during the Pliocene (Lisiecki and Raymo, 2005) and of stronger obliquity expression during low eccentricity intervals (Hilgen, 1991; 405-kyr minimum between cycles 9 and 8, Fig. 3D), but may not have been understood fully yet, as 41-kyr obliquity variation itself is at a minimum at this time (Fig. 3F).

4.3.4. Early Pleistocene orbital forcing

Comparable to the early Pliocene N14b-c boundary at ~4.6 Ma, the Ib-N16b-17a boundary at ~2.55 Ma is sitting in the middle of a 2.4-Myr eccentricity minimum (between cycles 1–2) close to a 405-kyr maximum (cycle 7, Fig. 3D). The boundary is also associated with maximum obliquity variation (1.2-Myr obliquity cycle 3, Fig. 3F). Strong 41-kyr obliquity minima associated with reduced summer insolation are considered critical moments for NH polar ice growth (e.g., Lourens and Hilgen, 1997). A strong 41-kyr obliquity minimum of 22.06° at 2.49 Ma, which slightly postdates the Ib-N16b-17a transition (2.54–2.56 Ma), correlates to MIS 100, which, together with the ensuing MIS 98 and 96 represent the first set of strong $\delta^{18}O$ events associated with NH glaciation. The occurrence of strong glacial events during intervals of maximum obliquity variation seems to be foreshadowed by the occurrence of events Si4–6 at 4.9 Ma during the previous strong obliquity antinode (cycle 5, Fig. 3F), when NH ice sheets were still in an ephemeral state (Zachos et al., 2001a).

The orbital configuration at the subsequent Ib-17a-17b boundary (between 2.15 and 2.05 Ma) reiterates orbital configurations at 6.95 and 4.0 Ma, with the boundary age uncertainty interval including a 405-kyr eccentricity minimum at the younger fringe of a 2.4-Myr minimum. Here, we consider a correlation to the strong 100/405-kyr minimum between cycles 6 and 5 at 2.07 Ma more probable than the correlation to the preceding, sub-maximal 100-kyr maximum at 2.12 Ma (Fig. 3D).

The orbital configuration at the top of Ib-N17b (1.9–1.8 Ma), on the other hand, resembles that of older Pliocene boundaries, such as Ib-N14c-15a and N16a-b in its association with a 1.2-Myr obliquity node and a 405-kyr eccentricity maximum (cycle 5, Fig. 3D) as well as with a distinct Mediterranean $\delta^{13}C$-$\delta^{18}O$ depletion event (Table 2). The occurrence of more humid conditions associated with these older Pliocene transitions also characterizes the 1.9–1.8 Ma interval, which at least partly corresponds to the 'Tiglian' interglacial (Zagwijn, 1992); top dated at ~1.8 Ma; Pillans and Gibbard, 2012). Immediately afterwards, SST starts to fluctuate strongly around 1.85–1.8 Ma in the North Atlantic and particularly in the Mediterranean, reaching peaks significantly cooler than before (Fig. 3A). Because precise age control is lacking, it is uncertain whether the immigration of rootless voles (including *Allophaiomys*) that defines the top of Ib-N17b occurred in association with relatively warm or cold conditions (for a discussion: see Repenning et al., 1990). Regardless of the climatic mode, the evolutionary novelty of ever-growing molars has allowed these voles to increase the per lifetime consumption of calory-poor bulk food and to be well prepared for a survival in the harsher environments that accompany Pleistocene glacials.

4.4. Synthesis: Biozone boundaries and dominant forcing mechanisms

The previous discussion shows that the timing of Iberian rodent zone boundaries can best be explained as the result of a series of changes in regional/Mediterranean humidity. Most of these changes are astronomically controlled and can be linked to extreme configurations of the 405-kyr and 2.4-Myr eccentricity cycle and the 1.2-Myr obliquity cycle (Table 2). Long biozones (i.e., 'no change', Ib-N11, N13c and N15b) occur during 2.4-Myr eccentricity maxima that concur with weak maxima in obliquity variation (8, 6, 4; Fig. 3F). During the late Miocene and earliest Pliocene (up to ~4.8 Ma) eccentricity appears to be the dominant parameter, with zone boundaries restricted to 405-kyr minima at 7.7, 6.9 and 4.9 Ma, and possibly also 6.5 and 5.4 Ma. These five boundaries are all positioned within broad 2.4-Myr eccentricity minima (characterized by weak 100-kyr eccentricity cycles) between cycles 4 and 3 (8–6.5 Ma) and between 3 and 2 (after 5.3 Ma; Fig. 3D). The role of obliquity seems subsidiary at this time; although the 7.7, ~6.5 and 5.4 Ma zone boundaries coincide with 1.2-Myr nodes, no boundaries occur at the onset or middle of the ~8.2–7.7 Ma node (cycle 8–7) or onset or middle of strong variation in the next antinode at 7.5–7.3 Ma (cycle 7). The typical climatic condition associated with late Miocene 405-kyr and 1.2-Myr minima is one of reduced humidity.

After ~4.8 Ma, faunal change is still associated with low eccentricity as dictated by 2.4-Myr eccentricity minima (weak 100-kyr cyclicity between 5.4 and 4.0 and 3.2–1.8 Ma) but the phase relationship with the 405-kyr cycle is reversed, with zone boundaries at 4.6, 4.2, possibly 3.9, 3.2, 3.0 Ma and 1.8 Ma associated with (wetter) maxima instead of (drier) minima. The 405-kyr eccentricity cycle thus affects the Iberian hydrological cycle in a consistent way at least from the late middle Miocene onwards with dry conditions occurring during minima (Sierro et al., 2000; Abdul Aziz et al., 2003; Hui et al., 2023). However, the correlation between Plio-Pleistocene zone boundaries and obliquity is much more pronounced than for late Miocene zone boundaries, with each of the three 1.2-Myr nodes around 4, 3 and 2 Ma corresponding to two separate zone boundaries, and the strong antinodes at ~5.0 and ~2.5 Ma associated with a zone boundary as well. Unlike the 405-kyr eccentricity cycle, but like the 2.4-Myr eccentricity cycle, the 1.2-Myr obliquity cycle changes its phase relationship with hydrology around the Miocene-Pliocene transition.

Although we regard climate change as the dominant agent in the pacing of terrestrial fauna, tectonic changes will additionally have affected the communities at times (Table 2). Especially during the Tortonian-Messinian transition (7.5–6.7 Ma), major tectonic activity (uplift and volcanism related to the alpine orogenesis; Krijgsman et al., 2018; Valla et al., 2012; Section 4.2.1) will have created environmental gradients and barriers preventing faunal exchange, subsequently leading to increased endemism and extinction (e.g., Zone Ib-N12b, van Dam et al., 2023). In addition, new physical migration routes were created as

a result of tectonic activity in the western peri-Mediterranean region, facilitating faunal exchange between Africa and Iberia (e.g., *Paraethomys* entry at base Ib-N13c) or possibly across desiccated areas (*Celadensia* at base Ib-N14a during the Messinian Salinity Crisis).

Here, we suggest that the shift in key orbital configurations affecting the fauna is linked to the late Neogene cooling trend controlling the position of the subtropical high-pressure zone in between the low-pressure tropical and temperate zones. With high-latitude climate forcing becoming more and more important during the Neogene (Westerhold et al., 2020; De Vleeschouwer et al., 2020) the Mediterranean region is expected to undergo a net transition from a subtropical warm and dry Miocene climate via a more temperate and less arid Pliocene climate to a cooler Pleistocene climate characterized by glacial (dry)- and interglacial (less dry) alternations (e.g., Tzedakis, 2007). Our observed shift from 405-kyr eccentricity minima to maxima as key moments for faunal change correlates in time to the reversal in phase around 4.5 Ma between global deep-sea $\delta^{13}C$ and $\delta^{18}O$ at the 100 and 405-kyr eccentricity scale as observed for the Atlantic Ocean (transition between climate – carbon cycle intervals II-III of De Vleeschouwer et al. (2020)). This reversal is attributed to a shift from net terrestrial carbon storage to net loss during eccentricity minima as the result of the global increase of less productive high-latitude biomes. In line with this scenario of global terrestrial productivity decrease and net aridification (with most change occurring at high latitudes and mid-continent areas), subtropical belts (which include the Iberian Peninsula) may have become temporarily more humid (Pliocene), because of the equatorward movement of the temperate belt.

At first sight, the correspondence of long periods of strongly fluctuating 100-kyr eccentricity (during 2.4-Myr eccentricity maxima; cycles 4, 3, 2; Fig. 3D) to long biozones (Ib-N11, N13c, 15b) is counterintuitive. On the one hand, obliquity could play a role, because extreme 41-kyr minima or maxima are not reached during these intervals (weak 1.2-Myr amplitude cycles 8, 6, 4; Fig. 3F). However, the question remains why strong 100-kyr eccentricity cycles and associated precessional changes had no disruptive effects on the fauna, despite a larger contribution of precession to insolation compared to obliquity at mid-latitudes (Milankovitch, 1930; Berger, 1978). The lack of such response either means that environments did not change on shorter time scales of 100 kyr or less (which is hard to believe and disproven by the literature on astronomically forced climate) or that species were somehow resilient to such shorter-lasting climate swings.

In the case of rodents, we previously suggested that buffering by short-distance (within-bioprovince) migration and recurrent amalgamation of incipient species with mother species could prevent long-term change (van Dam et al., 2006). Here, we extend this theoretical framework by assuming that immigration of new species from other bioprovinces constitutes the key disruptive factor in explaining faunal change at longer time scales. In this view, successful dispersal is only possible as a result of environmental changes that have sufficient magnitude and duration across areas sufficiently large and homogeneous (in terms of vegetation) in order to be crossed successfully. We postulate that only longer cycles such as the 405-kyr and 2.4-Myr eccentricity cycle and the 1.2-Myr obliquity cycle lead to the creation of such semi-permanent migration corridors that can be crossed by new immigrant species in large enough numbers in order to successfully outcompete the sitting species.

The relative insignificance of high-latitude forcing of the Iberian fauna during the latest Miocene and parts of the Pliocene should not be seen as evidence of for an absence of such forcing in older periods. For instance, most middle to late Miocene oxygen isotope ('Mi') events primary have been correlated to extreme points of long-period cycles in obliquity and eccentricity via SH glaciation (e.g., Lourens and Hilgen, 1997; Turco et al., 2001; Zachos et al., 2001b) and to Iberian rodent turnover (van Dam et al., 2006). Our observations confirm previous ideas that the latest Miocene - Pliocene constituted a special interval in between a period when either SH ice sheets (Oligocene to late Miocene, i.e., before Antarctica was more or less fully glaciated) or NH ice sheets (latest Pliocene-Pleistocene) were very dynamic (Zachos et al., 2001a; Rohling et al., 2021). During the early-middle Miocene, the effects of large fluctuations of the Antarctic ice sheet could have affected Northern Hemisphere climate via northward climate belt shifting (e.g., John et al., 2003; Holbourn et al., 2010), with the most extreme responses occurring during the Mi glacial/cooling events. Low-amplitude eccentricity and obliquity variation around 7.6 Ma may thus have been one of the last expressions of this typical Oligo-Miocene 'teleconnection mechanism' (MTi4 glacial event; Westerhold et al., 2005; Fig. 3B).

4.5. Stepwise clade displacement

From a macroevolutionary point of view, the fossil record consists of phylogenetic units (clades) that are continuously replacing each other (e.g., see: Fraser et al., 2021). Competing views on the underlying processes range between passive mechanisms rooted in the opportunistic diversification of surviving groups after extinction ('clade replacement'; Gould and Calloway, 1980; Benton, 1996) to active mechanisms rooted in ecological-time, inter-species competition ('clade displacement'; Sepkoski, 1996; Kemp, 2006). To judge whether clades competed or not, specific test criteria, such as stratigraphic overlap, inverse correlation in diversity and abundance ('double wedge'), and utilization of common resources can be used (Benton, 1996; Krause, 1986).

In our case, true mice and hamsters (indicated as 'clade group A') are replaced by vole-like hamsters and voles (indicated as 'clade group B', Fig. 2A,B). A and B share two major ecological properties (e.g., Nowak, 1999) that allow us as to regard these groups as potential competitors: 1) a similar locomotor style (terrestrial) and body size, although also aquatic adaptations occur in B, and 2) a dominantly vegetarian diet, although A is more specialized towards granivory and B towards herbivory. In terms of preferred climate, A is optimally adapted to the warm and dry subtropics, and B to the cooler and wetter temperate zone (Pliocene) or colder and drier boreal zone (Pleistocene). The observed stratigraphic overlap in combination with negatively correlated diversity/abundance patterns of the four major murid groups (Murinae, Cricetinae, Arvicolinae and 'microtoid cricetids', Fig. 2A,B) points to active competitive displacement.

But how is competition scaling down to the level of individual lineages? On the one hand, intra-clade competition is expected to be stronger than inter-clade competition because members of the same clade are closer phylogenetically. On the other hand, members of a newly arriving clade may possess key innovative features that work to their evolutionary-ecological advantage. In our case we suggest that a slow environmental change as ultimately guided by late Cenozoic cooling constituted the crucial background process driving clade displacement. During this gradual change, clade group B replaces group A in a stepwise fashion, with the steps being dictated by extremes of long-period Milankovitch cycles. The new group B takes over, because its clade members are better adapted to the changing conditions that more and more resemble those in their area of origin.

Due to the persistence of a warm and dry Miocene climate and a lack of suitable migration corridors, well-adapted resident groups such as true mice and hamsters could retain their dominant role in the late Miocene Iberian fauna. Because of their dominance, most lineage events could only take place within these groups during any upcoming perturbation. When paleoclimatic conditions changed in the Pliocene (with mid-latitude Atlantic sea surface temperatures dropping from 27 to 28 to ~20 °C; Fig. 3A), southern Europe climatically 'migrated' out of the warm subtropics into a mixed subtropical dry - temperate wet zone. We suggest that during humid 405-kyr eccentricity maxima and 1.2-Myr obliquity minima (Table 2) new, periodically functioning migration corridors were created across central and southern Europe. These routes acted as 'filters' across areas that previously were too arid to be successfully traversed by northern and eastern forms (see Brown and Lomolino, 1998, for a discussion on dispersal barriers). The immigration

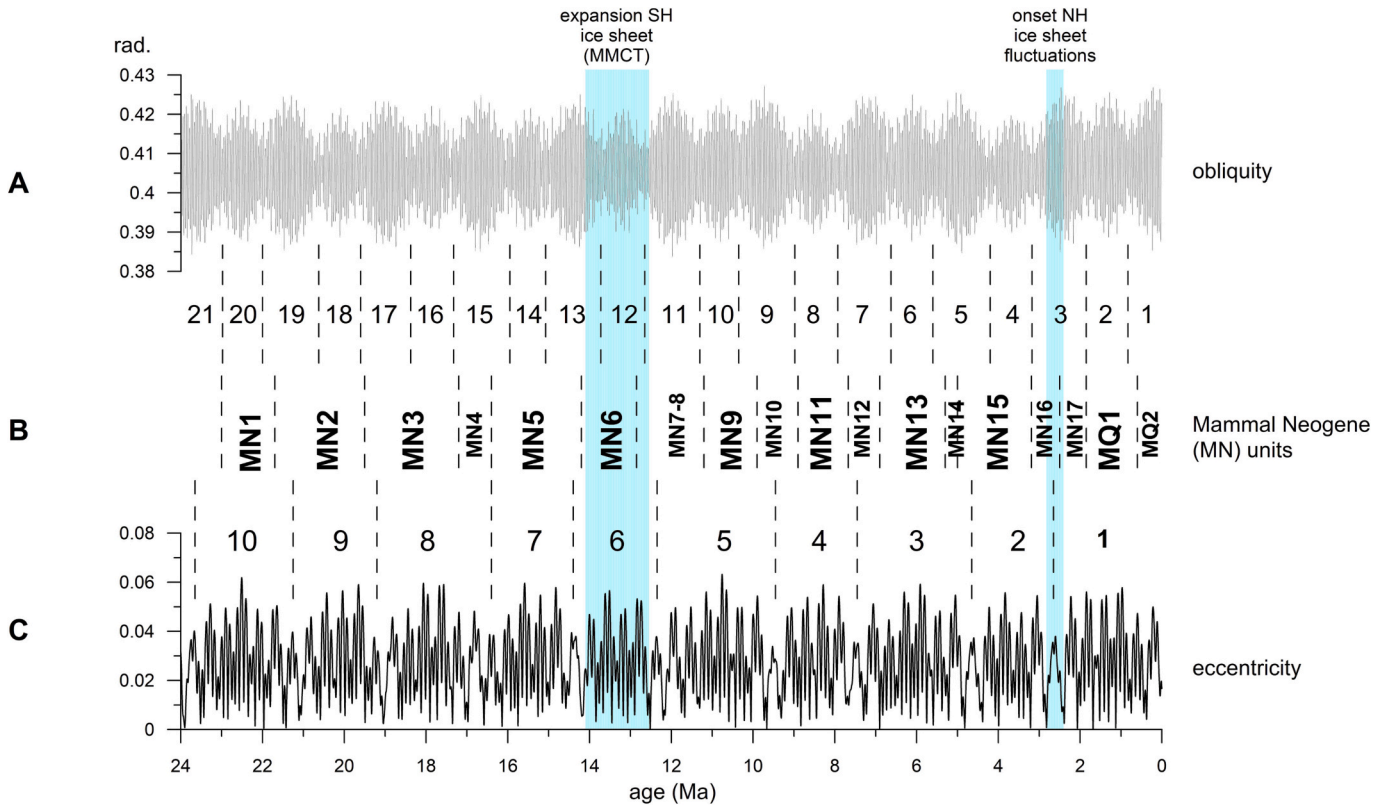

Fig. 4. Correlation between European Mammal Neogene (MN) and Quaternary (MQ) units and orbital parameters (obliquity, eccentricity; Laskar et al., 2004; astrochronozone numbering after Hilgen et al., (2020)). MMCT: middle Miocene climate transition. (A) Obliquity record. (B) MN units (Mein, 1975, 1990) and MQ units with boundaries corresponding to selected First Historical Appearance events (Hilgen et al., 2012). (C) Eccentricity record.

waves of eastern European microtoid hamsters and voles during the Iberian Pliocene (*Celadensia, Trilophomys*, *Mimomys davakosi*, *Dolomys*, *Mimomys hassiacus*) could be explained this way. (As noted above, Mediterranean desiccation may have additionally helped *Celadensia* in reaching Spain). Several of these waves have the actual form of an invasion, i.e., as an abundance peak event followed by a decline (for instance, *Mimomys davakosi*, *Dolomys adroveri*, *M. hassiacus*; Fig. 2C, Section 3.1.2). As one would expect, central parts of the Iberian Peninsula were colonized earlier and more extensively than the southern parts by most of these immigrants.

With global temperatures dropping another time in the early Pleistocene, Iberian voles were well prepared for these new conditions, given their area of origin (Asia) with its continental climate and low (winter) temperatures. Having become the new main residents in the Iberian Peninsula, evolutionary/radiational events started to outweigh immigrations also in the arvicoline clade, as evidenced by the development of endemic lineages (*Mimomys medasensis*, *M. realensis*, and *Kislangia gusii*). The short interval of endemic vole evolution corresponding to Zones Ib-N16b to 17b, was terminated by another immigration event that was part of a major expansion of a new type of voles (rootless voles, *Allophaiomys* event) across the Holarctic at 1.9–1.8 Ma.

The above model can easily be extended to other terrestrial mammals, as it only requires two groups adapted to different climate zones, a climatic trend, and ever-present Milankovitch cycles. For instance, a comparable case of clade 'displacement' (i.e., active replacement) has been described involving the substitution of pelycosaurs by therapsids during the Permian (Kemp, 2006). Although Milankovitch cycles (which also existed hundreds of million years ago with short as well as long periods; Olsen and Kent, 1999) were not included in that study, resource utilization and shifting climate zones are thought to have played a crucial role.

An alternative clade replacement model, in which extinction precedes immigration and radiation (the 'incumbent replacement' model of Rosenzweig and McCord, 1991), does not apply very well to our case. This model, which functions particularly well in the context of mass extinctions, may not be very suitable to explain 'mainstream' (sub) family-level replacements that shape the fossil record at the 10^{6-7}-million-year scale. In our model, 'incumbency' (i.e., the power of 'simply being there first') is still an important concept, however. At the lineage level, this concept applies to the long intervals of rapidly oscillating ~21-kyr precession and 41-kyr obliquity, during which successful immigrations of new forms largely fail. At the clade-level, incumbency applies to the middle part of our group A clade history, when most lineages involved in replacements simply belong to the same clades (true mice and hamsters). Here, "privileges of incumbency (including substantial geographic range, large numbers of organisms and multiple species, heavy use of resources preventing new taxa from gaining a foothold) buffer existing taxa against the slowly changing conditions." (Gilinsky and Bambach, 1987: p444). However, in the post-bloom part of our clade A (Plio-Pleistocene), geographical range boundaries are breached during critical phases (400-kyr eccentricity maxima; 1.2-Myr obliquity minima) and faunal composition changes. Metaphorically, one could say that it needs multiple 'sieges' at the right moments to finally 'conquer' the 'enemy's' territory. As Gilinski and Bambach note from the perspective of the conquered clade: "Thus, as time passes, the group's genetic and developmental system becomes increasingly removed from the context in which it arose, and increasingly fewer branching events lead to successful establishment of new species and families".

4.6. Astronomical pacing of European Mammal Neogene (MN) units

Fig. 3 suggests an astronomical origin for larger-scale biochronological units as well, with MN12, MN14 and MN16–17

corresponding to periods of low average eccentricity (2.4-Myr cycle) and strong obliquity amplitude maxima (1.2-Myr cycle), and MN11, MN13 and MN15 associated with high average eccentricity and weak obliquity amplitude maxima.

When the complete set of Neogene MN units is inspected (Fig. 4), the association with long-period orbital cycles becomes even more evident. Whereas the sequence of early to early middle (pre-14 Ma) Miocene units MN1–5 temporally correlates to 2.4-Myr eccentricity cycles 10–7 on an almost one-to-one basis (the placement of the short MN4 between the longer MN3 and MN5 is an exception), the sequence of post-14 Ma units from MN6 onwards correlates on a one-to-one basis to the 1.2-Myr obliquity cycles 11–1. The only exception here is the temporal correspondence of two units (MN16 and 17) to one cycle (no. 3), of which the maximum amplitude point corresponds to their boundary as well as to the Neogene-Quaternary boundary.

The tight correlation between astronomical cycles and MN units is all the more remarkable, as the latter were defined about fifty years ago based on faunal content only (Mein, 1975, 1990). At that time, calibrations to the geological time scale were still poor and there was no knowledge of orbital forcing of faunas on a million-year time scale. Although the definition of MN units is not without problems (Hilgen et al., 2012), discussions have mainly focused on boundaries rather than on contents or number of units. In this respect it should be noted that the boundaries between MN units as drawn in Fig. 4 should not be treated as moments of sudden fauna-wide turnover. Rather, most of the boundary definitions depend on choices for specific appearance events, which may or may not be isochronous with other (dis)appearance events. (A concrete example is the choice of the *Mimomys* entry as base for MN15, resulting in a very short MN14 unit, Fig. 4; Hilgen et al., 2012.) In fact, the gradual change from one continental-scale fauna to another is consistent with the slow change in long-period orbital parameters, to which species respond differently (although it is expected that unit transitions last much shorter than the units themselves).

It thus appears that the two major Neogene global climate transitions (mid-Miocene cooling transition (MMCT) with an expanding SH ice sheet around 14 Ma and the onset of NH-derived glacial-interglacial cycles around 2.5 Ma, Fig. 4; Zachos et al., 2001a; Westerhold et al., 2020; Rohling et al., 2021) also represent dividing points in the macroecological and macroevolutionary history of European mammals. The absence of a clear imprint of the 1.2-Myr obliquity cycle during the early-middle Miocene (before ~14 Ma, but especially before 17 Ma) is intriguing, as this cycle has repeatedly been encountered in the geological archive, including older Oligocene to middle Miocene benthic $\delta^{18}O$ records across the World's oceans, where obliquity nodes have been found to correspond to glacial episodes on Antarctica (Zachos et al., 2001b; Pälike et al., 2006). Apparently, European-scale faunal change during the early Miocene was mostly dependent on regional, eccentricity-precession-controlled climatic change, with high-latitude forcing (obliquity) playing a minor role. After the early-middle Miocene transition (17–16 Ma), and even more so after the mid-Miocene cooling event (14 Ma), a stronger obliquity influence on the Atlantic-Eurasian climate made itself felt. Given the amplification of insolation variations on land (Short et al., 1991; Seltzer et al., 2023) and the increasing importance of aridity and wet-dry variations continent-inward, the faunal replacement model as proposed here for late Neogene rodent clades could easily be extended to mammal faunas as a whole.

5. Conclusions

A comparison of late Miocene to early Pleistocene Iberian rodent biozone boundary ages with records of marine SST, $\delta^{18}O$ and $\delta^{13}C$, terrestrial hydrological proxies, and astronomical parameters suggests an orbital background for most zones, with specific configurations (minima, maxima) of the 1.2-Myr obliquity cycle and the 405-kyr/2.4-Myr eccentricity cycles controlling faunal changes via oscillations in Mediterranean humidity and vegetation. Pacing of larger-scale, Neogene European mammal chronological (MN) units by million-year-scale eccentricity and obliquity cycles is strongly suggested as well. Phase relationships between orbital parameters and environment/fauna are not constant, however, but depend on the state of the background climate. With climate belts moving equatorward during gradual late Neogene cooling, more and more rodent forms with a more temperate / higher-latitude origin ('microtoid hamsters' and voles) are successively introduced into the existing Mediterranean fauna dominated by true mice and hamsters. A new model of stepwise clade displacement is thus proposed in which a series of increasingly pervasive, orbitally forced dispersal events of the new clade gradually disrupts the supremacy of the old clade and leads to its gradual extinction.

Although an analysis of actual micromammal lineage turnover (sensu van Dam et al., 2006) is expected to give more detailed results, our correlations at the biozone level are specific enough to formulate several important implications for macroevolutionary/macroevolutionary theory:

1) Oscillations of long-term climatic parameters (notably the 405-kyr, 1.2-Myr and 2.4-Myr envelopes of shorter-term ~21-kyr, 41-kyr and ~ 100-kyr Milankovitch cycles) constitute an attractive mechanism for triggering background species-level and (sub)family-level evolution. Besides exerting a more direct influence via global cooling events (e.g., Pleistocene), these long cycles affect the connectivity between bioprovinces (by the expansion and shrinking of biome vegetation), affecting overall rates of animal migration and interspecific competition.
2) Evolutionary rates on the 10^{5-6}-year scale are higher during some intervals than others, because of the concentration in time of faunal events including the addition of new, competing species from remote areas (dispersal) and from nearby areas (local speciation following local extinction). Previous hypotheses (e.g., 'Turnover-pulse' and 'Court-Jester' hypotheses; Vrba, 1995; Barnosky, 2001) have stressed the importance of climatic triggers (including Milankovitch cycles) for evolution, focusing particularly on extreme global cooling/warming events. Our model is less demanding, stressing the importance of changes in regional insolation patterns as controlled by long-period Milankovitch cycles. In addition, the model includes long-term resilience to short-period climate change as a central component (e.g., Ivany, 1996), as a result of which permanent ecosystem changes only occur after relatively long (> ~ 100-kyr) intervals with deviating conditions.
3) The stepwise clade displacement model is relevant to theories of species radiation, because it predicts a concentration of speciation events in time (e.g., Eldredge and Gould, 1972).
4) The faunal dynamics model proposed here is relevant to macroecological theory, because it provides a time scale for species-level stasis (in aspects such as diversity, abundance, distribution; Brown and Lomolino, 1998; Rosenzweig and McCord, 1991), while acknowledging the importance of bioprovincial exchange and dispersal.

Admittedly, our study is limited to one group (rodents), abundance class (mostly common species), area (Iberian Peninsula), time frame (late Neogene) and data resolution type (no data at 10^{3-4}-year time scale). On the other hand, the approximately similar, 10^{5-6}-year-level duration of biozones in other marine and terrestrial realms across geological history (Gradstein et al., 2020) suggests that a similar type of forcing was at work. Obviously, much more testing will be necessary before astronomically forced climate change can be accepted as a prime cause for species and community turnover in the fossil record.

Declaration of Competing Interest

The authors declare that they have no known competing financial

interests or personal relationships that could have appeared to influence the work reported in this paper.

Data availability

Research data are attached in the Supplementary Tables accompanying this paper

Acknowledgments

We thank Raef Minwer Barakat for allowing us to use his quantitative data for Guadix-Baza Basin rodents and Tanja Kouwenhoven and Alexandrina Tzanova for their data from Mediterranean Sea records. Frits Hilgen and Gert-Jan Reichart are thanked for discussion and the reviewers for their comments. This publication is part of project I+D+i PID2020-117289GBI00 funded by MCIN/AEI/10.13039/501100011033. Our research has also been supported by CERCA Programme/Generalitat de Catalunya, AEI–FEDER EU (to M.F.), AGAUR (Consolidated Research Group, 2017 SGR 960 to M.F. and 2017 SGR 596 to M.G.), and the Department of Science, University and Society of Knowledge of the Government of Aragon (Reference Research Group E04_20R FOCONTUR funding to Fundación Dinópolis -L.A.).

Appendix A. Supplementary data

Supplementary data to this article can be found online at https://doi.org/10.1016/j.gloplacha.2023.104153.

References

Abdul Aziz, H., Sanz-Rubio, E., Calvo, J.P., Hilgen, F.J., Krijgsman, W., 2003. Paleoenvironmental reconstruction of a middle Miocene proximal alluvial fan to cyclic shallow lacustrine depositional system in the Calatayud Basin (NE Spain). Sedimentol. 50, 211–236.

Abdul Aziz, H., van Dam, J.A., Hilgen, F.J., Krijgsman, W., 2004. Astronomical forcing in Upper Miocene continental sequences: implications for the Geomagnetic Polarity Time Scale. Earth Planet. Sci. Lett. 222, 243–258.

Abels, H.A., Abdul Aziz, H., Calvo, J.P., Tuenter, E., 2008. Shallow lacustrine microfacies document orbitally paced lake-level history in the Miocene Teruel Basin (NE Spain). Sedimentol. 56, 399–419.

Abels, H.A., Aziz, H.A., Ventra, D., Hilgen, F.J., 2009. Orbital climate forcing in mudflat to marginal lacustrine deposits in the Miocene Teruel Basin (Northeast Spain). J. Sediment. Res. 79, 831–847.

Abels, H.A., Aziz, H.A., Krijgsman, W., Smeets, S.J.B., Hilgen, F.J., 2010. Long-period eccentricity control on sedimentary sequences in the continental Madrid Basin (middle Miocene, Spain). Earth Planet. Sci. Lett. 289, 220–231.

Abreu, V.S., Anderson, J.B., 1998. Glacial eustasy during the Cenozoic: sequence stratigraphic implications. AAPG Bull. 82, 1385–1400.

Adrover, R., Mein, P., Moissenet, E., 1993. Roedores de la transición Mio-Plioceno de la región de Teruel. Paleontol. Evol. 26-27, 47–84.

Agustí, J., Oms, O., Remacha, E., 2001. Long Plio-Pleistocene terrestrial record of climate change and mammal turnover in southern Spain. Quat. Res. 56, 411–418.

Agustí, J., Garcés, M., Krijgsman, W., 2006. Evidence for African-Iberian exchanges during the Messinian in the Spanish mammalian record. Palaeogeogr. Palaeoclimatol. Palaeoecol. 238, 5–14.

Alcalá, L., Alonso-Zarza, A., Álvarez Sierra, M.A., Azanza, B., Calvo, J.P., Cañaveras, J.C., van Dam, J., Garcés, M., Krijgsman, W., van der Meulen, A.J., Morales, J., Peláez-Campomanes, P., Pérez González, A., Sánchez Moral, S., Sancho, R., Sanz Rubio, E., 2000. El registro sedimentario y faunístico de las cuencas de Calatayud-Daroca y Teruel. Evolución paleoambiental y paleoclimática durante el Neógeno. Rev. Soc. Geol. Esp. 13, 323–343.

Alonso-Zarza, A.M., Calvo, J.P., 2000. Palustrine sedimentation in an episodically subsiding basin: the Miocene of the northern Teruel Graben (Spain). Palaeogeogr. Palaeoclimatol. Palaeoecol. 160, 1–21.

Barnosky, A.D., 2001. Distinguishing the effects of the Red Queen and Court Jester on Miocene mammal evolution in the northern Rocky Mountains. J. Vertebr. Paleontol. 21, 172–185.

Benson, R.H., Rakic-El Bied, K., Bonaduce, G., 1991. An important current reversal (influx) in the Rifian Corridor (Morocco) at the Tortonian-Messinian boundary: the end of Tethys Ocean. Paleoceanogr. 6, 165–192.

Benton, M.J., 1996. On the nonprevalence of competitive replacement in the evolution of tetrapods. In: Jablonski, D., Erwin, D.H., Lipps, J.H. (Eds.), Evolutionary Paleobiology. Chicago University Press, Chicago, pp. 185–210.

Berger, A.L., 1978. Long-term variations of caloric insolation resulting from the Earth's orbital elements. Quat. Res. 9, 139–167.

Böhme, M., Ilg, A., 2003. Database on fossil fishes, amphibians and reptiles: fosFARbase. http://www.wahre-staerke.com.

Bosmans, J., Drijfhout, S., Tuenter, E., Hilgen, F.J., Lourens, L.J., Rohling, E., 2015a. Precession and obliquity forcing of the freshwater budget over the Mediterranean. Quat. Sci. Rev. 123, 16–30.

Bosmans, J., Hilgen, F., Tuenter, E., Lourens, L.J., 2015b. Obliquity forcing of low-latitude climate. Clim. Past 11, 1335–1346.

Bosmans, J., van der Ent, R.J., Haarsma, R., Drijfhout, S.S., Hilgen, F.J., 2020. Precession- and obliquity-induced changes in moisture sources for enhanced precipitation over the Mediterranean Sea. Paleoceanogr. Paleoclimatol. 36, e2019PA003655 https://doi.org/10.1029/2019PA003655.

Brown, J.H., Lomolino, M.V., 1998. Biogeography. Sinauer Associates, Inc., Sunderland, Massachusetts.

Butiseaca, G.A., Vasiliev, I., van der Meer, M.T.J., Krijgsman, W., Palcu, D.V., Feurdean, A., Niedermeyer, E.M., Mulch, A., 2021. Severe late Miocene droughts affected western Eurasia. Glob. Planet. Chang. 206, 103644 https://doi.org/10.1016/j.gloplacha.2021.103644.

Calvo, J.P., Alcalá, L., Alonzo Zarza, A., van Dam, J.A., Gutiérrez Santolalla, F., 1999. Estratigrafía y structura del área de Los Mansuetos (Cuenca de Teruel). Precisiones para la definición del estratotipo del Turoliense. Geogac. 25, 55–58.

Casanovas-Vilar, I., Agustí, J., 2007. Ecogeographical stability and climate forcing in the late Miocene (Vallesian) rodent record of Spain. Palaeogeogr. Palaeoclimatol. Palaeoecol. 248, 169–189.

Channell, J.E.T., Amigo, A.E., Fronval, T., Rack, F., Lehman, B., 1999. Magnetic stratigraphy at Sites 907 and 985 in the Norwegian-Greenland Sea and a revision of the Site 907 composite section. In: Raymo, M.E., Jansen, E., Blum, P., Herbert, T.D. (Eds.), Proc. Ocean Drill. Program Sci. Res., 162 Ocean Drilling Program, College Station, Texas, pp. 131–148.

Chevret, P., Renaud, S., Helvaci, Z., Ulrich, R.G., Quéré, J.P., Michaux, J.R., 2020. Genetic structure, ecological versatility, and skull shape differentiation in *Arvicola* water voles (Rodentia, Cricetidae). J. Zool. Syst. Evol. Res. 58, 1323–1334.

Conte, M., Sicre, M.-A., Ruhlemann, C., 2006. Global temperature calibration of the alkenone unsaturation index ($U^{K'}37$) in surface waters and comparison with surface sediments. Geochem. Geophys. Geosyst. 7, Q02005. https://doi.org/10.1029/2005GC001054.

de Bruijn, H., Mein, P., Montenat, C., van de Weerd, A., 1975. Correlations entre les gisements de rongeurs et les formations marines du Miocène terminal d'Espagne meridionale; provinces d'Alicante et de Murcia. Proc. K. Ned. Akad. Wet. Ser. B 78, 282–313.

De Miguel, D., Azanza, B., Morales, J., 2019. Regional impacts of global climate change: a local humid phase in Central Iberia in a late Miocene drying world. Paleontol. 62, 77–92.

De Vleeschouwer, D., Drury, A.J., Vahlenkamp, M., Rochholz, F., Liebrand, D., Pälike, H., 2020. High-latitude biomes and rock weathering mediate climate-carbon cycle feedbacks on eccentricity timescales. Nat. Commun. 11, 1–10.

Drury, A.J., Westerhold, T., Frederichs, T., Tian, J., Wilkens, R., Channell, J.E.T., Evans, H., Johns, C.M., Lyle, M., Rohl, U., 2017. Late Miocene climate and time scale reconciliation: Accurate orbital calibration from a deep-sea perspective. Earth Planet. Sci. Lett. 475, 254–266.

Eldredge, N., Gould, S.J., 1972. Punctuated equilibria: analternative to phyletic gradualism. In: Schopf, T.J.M. (Ed.), Models in paleobiology. W. H. Freeman, San Francisco, pp. 82–115.

Ezquerro, L., Luzón, A., Simón, J.L., Liesa, C.L., 2020. Segmentation and increasing activity in the Neogene-Quaternary Teruel Basin rift (Spain) revealed by morphotectonic approach. J. Struct. Geol. 135, 104043 https://doi.org/10.1016/j.jsg.2020.104043.

Ezquerro, L., Muñoz, A., Liesa, C.L., Simón, J.L., Luzón, A., 2022. Late Neogene to early Quaternary climate evolution in southwestern Europe from a continental perspective. Glob. Planet. Chang. 211, 103788 https://doi.org/10.1016/j.gloplacha.2022.103788.

Fauquette, S., Guiot, J., Suc, J.-P., 1998. A method for climatic reconstruction of the Mediterranean Pliocene using pollen data. Palaeogeogr. Palaeoclimatol. Palaeoecol. 144, 183–201.

Fejfar, O., Heinrich, W.D., Kordos, L., Maul, L.C., 2011. Microtoid cricetids and the early history of arvicolids (Mammalia, Rodentia). Palaeontol. Electron. 14, 27A. https://palaeo-electronica.org/2011_3/6_fejfar/index.html.

Fraser, D., Soul, L.C., Tóth, A.B., Balk, M.A., Eronen, J.T., Pineda-Munoz, S., Shupinski, A.B., Villaseñor, A., Barr, W.A., Behrensmeyer, A.K., Du, A., Faith, J.T., Gotelli, N.J., Graves, G.R., Jukar, A.M., Looy, C.V., Miller, J.H., Potts, R., Lyons, S.K., 2021. Investigating biotic interactions in deep time. Trends Ecol. Evol. 36, 61–75.

Freudenthal, M., Mein, P., Martín Suárez, E., 1998. Revision of late Miocene and Pliocene Cricetinae (Rodentia, Mammalia) from Spain and France. Treb. Mus. Geol. Barc. 7, 11–93.

Gao, P., Nie, J., Breecker, D.O., Gallagher, T., Serach, L., Alonso- Zarza, A.M., 2022. Similar magnetic enhancement mechanisms between Chinese loess and alluvial sediments from the Teruel Basin, NE Spain, and paleoclimate implications. Geophys. Res. Lett. 49, e2021GL096977 https://doi.org/10.1029/2021GL096977.

Garcés, M., Krijgsman, W., Agustí, J., 2001. Chronostratigraphic framework and evolution of the Fortuna basin (Eastern Betics) since the late Miocene. Basin Res. 13, 199–216.

Gilinsky, N.L., Bambach, R.K., 1987. Asymmetrical patterns of origination and extinction in higher taxa. Paleobiol. 13, 427–445.

Godoy, A., Olivé, A., Moissenet, E., 1983. Mapa y memoria explicativa de la Hoja 567 (Teruel) del Mapa Geológico de España, a escala 1:50.000 (2a Serie). IGME Madrid, 1-70.

Gould, S.J., Calloway, C.B., 1980. Clams and brachiopods: ships that pass in the night. Paleobiol. 6, 383–396.

Gradstein, F.M., Ogg, J.G., Schmitz, M.D., Ogg, G.M., 2020. The Geologic Time Scale 2020, 2. Elsevier, Boston, MA.
Gudjonsson, L., van der Zwaan, G.J., 1985. Anoxic events in the Pliocene Mediterranean: stable isotope evidence of run-off. Proc. K. Ned. Akad. Wet. Ser. B 88, 69–82.
Gusovsky, V.V., Sinitsa, M.V., 2021. Dietary preferences and autecology of a basal Holarctic ground squirrel *Spermophilinus* (Rodentia: Sciuridae: Xerinae), inferred from dental microwear analysis. Hist. Biol. 33, 54–61.
Henderson-Sellers, A., Robinson, P.J., 1994. Contemporary Climatology. John Wiley & Sons, New York.
Herbert, T.D., Lawrence, K.T., Tzanova, A., Peterson, L.C., Caballero-Gill, R., Kelly, C.S., 2016. Late Miocene global cooling and the rise of modern ecosystems. Nat. Geosci. 9, 843–849.
Herold, N., Muller, R.D., Seton, M., 2010. Comparing early to middle Miocene terrestrial climate simulations with geological data. Geosph. 6, 952–961.
Hilgen, F.J., 1991. Extension of the astronomically calibrated (polarity) time scale to the Miocene/Pliocene boundary. Earth Planet. Sci. Lett. 107, 349–368.
Hilgen, F.J., Lourens, L.J., van Dam, J.A., 2012. The Neogene Period. In: Gradstein, F.M., Ogg, J.G., Schmitz, M.D., Ogg, G. (Eds.), A geological time scale 2012. Elsevier, Amsterdam, pp. 923–978.
Hilgen, F.J., Lourens, L.J., Pälike, H., Research Support Team, 2020. Should unit-stratotypes and astrochronozones be formally defined? A dual proposal (including postscriptum). Newsl. Stratigr. 53, 19–39.
Hodell, D.A., Benson, R.H., Kennett, J.P., Rakic-El Bied, K., 1989. Stable isotope stratigraphy of latest Miocene sequences in Northwest Morocco: the Bou Regreg Section. Paleoceanogr. 4, 467–482.
Hodell, D.A., Benson, R.H., Kent, D.V., Boersma, A., Bied, K.R.E., 1994. Magnetostratigraphic, biostratigraphic, and stable-isotope stratigraphy of an upper Miocene drill core from the Salé-Briqueterie (northwestern Morocco): a high-resolution chronology for the Messinian stage. Paleoceanogr. 9, 835–855.
Hodell, D.A., Curtis, J.H., Sierro, F.J., Raymo, M.E., 2001. Correlation of late Miocene to early Pliocene sequences between the Mediterranean and North Atlantic. Paleoceanogr. 16, 164–178.
Holbourn, A., Kuhnt, W., Regenberg, M., Schulz, M., Mix, A., Andersen, N., 2010. Does Antarctic glaciation force migration of the tropical rain belt? Geology 38, 783–786.
Hordijk, K., de Bruijn, H., 2009. The succession of rodent faunas from the Mio/Pliocene lacustrine deposits of the Florina-Ptolemais-Servia Basin (Greece). Hell. J. Geosci. 44, 21–103.
Hui, Z., Liu, J., Chevalier, M., Wei, X., Chen, P., Zhang, J., Peng, T., Zhou, X., 2023. Multiple forcing on late Miocene East Asian Summer Monsoon Precipitation Variability in NE Tibetan Plateau. Catena 221 A, 106752. https://doi.org/10.1016/j.catena.2022.106752.
Ivany, L.C., 1996. Coordinated stasis or coordinated turnover? Exploring intrinsic vs. extrinsic controls on pattern. Palaeogeogr. Palaeoclimatol. Palaeoecol. 127, 239–256.
Jardine, P.E., Janis, C.M., Sahney, S., Benton, M.J., 2012. Grit not grass: concordant patterns of early origin of hypsodonty in Great Plains ungulates and Glires. Palaeogeogr. Palaeoclimatol. Palaeoecol. 365, 1–10.
John, C.M., Mutti, M., Adatte, T., 2003. Mixed carbonate-siliciclastic record on the North African margin (Malta) - coupling of weathering processes and mid Miocene climate. Geol. Soc. Am. Bull. 115, 217–229.
Kälin, D., Kempf, O., 2009. High-resolution stratigraphy from the continental record of the Middle Miocene Northern Alpine Foreland Basin of Switzerland. N. Jahrb. Geol. Paläontol. Abh. 254, 177–235.
Kemp, T.S., 2006. The origin and early radiation of the therapsid mammal-like reptiles: a palaeobiological hypothesis. J. Evol. Biol. 19, 1231–1247.
Kloosterboer - van Hoeve, M., 2000. Cyclic changes in the late Neogene vegetation of northern Greece. LPP Contrib. Ser. 12, 1–131.
Kontakiotis, G., Besiou, E., Antonarakou, A., Zarkogiannis, S.D., Kostis, A., Mortyn, P.G., Moissette, P., Cornée, J.-J., Schulbert, C., Drinia, H., Anastasakis, G., Karakitsios, V., 2022. Decoding Sea surface and paleoclimate conditions in the eastern Mediterranean over the Tortonian-Messinian transition. Palaeogeogr. Palaeoclimatol. Palaeoecol. 534, 109312.
Kouwenhoven, T.J., van der Zwaan, G.J., 2006. A reconstruction of late Miocene Mediterranean circulation patterns using benthic foraminifera. Palaeogeogr. Palaeoclimatol. Palaeoecol. 238, 373–385.
Kouwenhoven, T.J., Seidenkrantz, M.-S., van der Zwaan, G.J., 1999. Deep-water changes: the near-synchronous disappearance of a group of benthic foraminifera from the late Miocene Mediterranean. Palaeogeogr. Palaeoclimatol. Palaeoecol. 152, 259–281.
Krause, D.W., 1986. Competitive exclusion and taxonomic displacement in the fossil record: The case of rodents and multituberculates in North America. In: Flanagan, K. M., Lillegraven, J.A. (Eds.), Vertebrates, Phylogeny, and Philosophy. University of Wyoming, Laramie.
Krijgsman, W., Hilgen, F.J., Raffi, I., Sierro, F.J., Wilson, D.S., 1999. Chronology, causes and progression of the Messinian salinity crisis. Nature 400, 652–655.
Krijgsman, W., Capella, W., Simon, D., Hilgen, F.J., Kouwenhoven, T.J., Sierro, F.J., Tulbure, M.A., van den Berg, B.C.J., van der Schee, M., Rachel Flecker, R., 2018. The Gibraltar Corridor: watergate of the Messinian Salinity Crisis. Mar. Geol. 403, 236–246.
Kuiper, K.F., Krijgsman, W., Garcés, M., Wijbrans, J., 2006. Revised isotopic (40Ar/39Ar) age for the lamproite volcano of Cabezos Negros, Fortuna Basin (Eastern Betics, SE Spain). Palaeogeogr. Palaeoclimatol. Palaeoecol. 238, 53–63.
Kutzbach, J.E., Chen, G., Cheng, H., Edwards, R.L., Liu, Z., 2014. Potential role of winter rainfall in explaining increased moisture in the Mediterranean and Middle East during periods of maximum orbitally-forced insolation seasonality. Clim. Dyn. 42, 1079–1095.
Laskar, J., Robutel, P., Joutel, F., Gastineau, M., Correia, A.C.M., Levrard, B., 2004. A long-term numerical solution for the insolation quantities of the Earth. Astron. Astrophys. 428, 261–285.
Lawrence, K.T., Herbert, T.D., Brown, C.M., Raymo, M.E., Haywood, A.M., 2009. High-amplitude variations in North Atlantic Sea surface temperature during the early Pliocene warm period. Paleoceanogr. 24, PA2218.
Lisiecki, L.E., Raymo, M.E., 2005. A Pliocene-Pleistocene stack of 57 globally distributed benthic $\delta^{18}O$ records. Paleoceanogr. 20, PA001071. https://doi.org/10.1029/2004PA001071.
López-Martínez, N., 1989. Revisión sistemática y biostratigráfica de los lagomorfos (Mammalia) el Terciario y Cuaternario inferior de España. Diputación General de Aragón, Zaragoza.
Lourens, L.J., Hilgen, F.J., 1997. Long-periodic variations in the earth's obliquity and their relation to third-order eustatic cycles and late Neogene glaciations. Quat. Int. 40, 43–52.
Lourens, L.J., Hilgen, F.J., Gudjonsson, L., Zachariasse, W.J., 1992. Late Pliocene to early Pleistocene astronomically forced sea surface productivity and temperature variations in the Mediterranean. Mar. Micropaleontol. 19, 49–78.
Lourens, L.J., Hilgen, F.J., Antonarakou, A., Van Hoof, A.A.M., Vergnaud-Grazzini, C., Zachariasse, W.J., 1996. Evaluation of the Pliocene to early Pleistocene astronomical time scale. Paleoceanogr. 11, 391–413.
Martin, R.A., 2008. Arvicolidae. In: Janis, C.M., Gunnell, G.F., Uhen, M.D. (Eds.), Evolution of Tertiary Mammals of North America, vol. 2. Cambridge University Press, Cambridge, pp. 480–497.
Martín Suárez, E., Mein, P., 1998. Revision of the genera *Parapodemus*, *Apodemus*, *Rhagamys* and *Rhagapodemus* (Rodentia, Mammalia). Geobios 31, 87–97.
Mein, P., 1975. Résultats du Groupe de Travail de Vertébrés. In: Senes, J. (Ed.), Report on Activity of the RCMNS Working Groups (1971–1975). RCMNS, Bratislava, pp. 78–81.
Mein, P., 1990. Updating of MN zones. In: Lindsay, E., Fahlbusch, V., Mein, P. (Eds.), European Neogene Mammal Chronology. NATO ASI Series A, pp. 73–90.
Mein, P., Moissenet, E., Adrover, R., 1990. Biostratigraphie du Neogène supérieur du bassin de Teruel. Paleontol. Evol. 23, 121–139.
Milankovitch, M., 1930. Mathematische Klimalehre und astronomische Theorie der Klimaschwankungen. In: Köppen, W., Gieger, R. (Eds.), Handbuch der Klimatologie I (A), pp. 1–176.
Nobel, F.A., Andriessen, P.A.M., Hebeda, E.H., Priem, H.N.A., Rondeel, H.E., 1981. Isotopic dating of the post-alpine Neogene volcanism in the Betic Cordilleras, Southern Spain. Geol. Mijnb. 60, 209–214.
Nowak, R.M., 1999. Walkers' Mammals of the World. Johns Hopkins University Press, Baltimore.
Olsen, P.E., Kent, D.V., 1999. Long-period Milankovitch cycles from the late Triassic and early Jurassic of eastern North America and their implications for the calibration of the early Mesozoic time-scale and the long-term behaviour of the planets. Philos. Trans. R. Soc. Lond. A 357, 1761–1786.
Opdyke, N., Mein, P., Lindsay, E., Pérez-Gonzáles, A., Moissenet, E., Norton, V.L., 1997. Continental deposits, magnetostratigraphy and vertebrate paleontology, late Neogene of Eastern Spain. Palaeogeogr. Palaeoclimatol. Palaeoecol. 133, 129–148.
Palcu, D.V., Vasiliev, I., Stoica, M., Krijgsman, W., 2019. The end of the Great Khersonian Drying of Eurasia: magnetostratigraphic dating of the Maeotian transgression in the Eastern Paratethys. Basin Res. 31, 33–58.
Palcu, D.V., Patina, I.S., Sandric, I., Lazarev, S., Vasiliev, I., Stoica, M., Krijgsman, W., 2021. Late Miocene megalake regressions in Eurasia. Sci. Rep. 11, 11471.
Pälike, H., Norris, R.D., Herrle, J.O., Wilson, P.A., Coxall, H.K., Lear, C.H., Shackleton, N. J., Tripati, A.K., Wade, B.S., 2006. The heartbeat of the Oligocene climate system. Science 314, 1894–1898.
Panitz, S., Salzmann, U., Risebrobakken, B., De Schepper, S., Pound, M.J., 2016. Climate variability and long-term expansion of peat lands in Arctic Norway during the late Pliocene (ODP Site 642, Norwegian Sea). Clim. Past 12, 1043–1060.
Pillans, B., Gibbard, P., 2012. The Quaternary Period. In: Gradstein, F.M., Ogg, J.G., Schmitz, M.D., Ogg, G. (Eds.), A Geological Time Scale 2012. Elsevier, Amsterdam, pp. 979–1010.
Qin, J., Zhang, R., Kravchinsky, V.A., Valet, J.-P., Sagnotti, L., Li, J., Xu, Y., Anwar, T., Yue, L., 2022. 1.2 Myr band of Earth-Mars obliquity modulation on the evolution of cold late Miocene to warm early Pliocene climate. J. Geophys. Res. Solid Earth 127, e2022JB024131. https://doi.org/10.1029/2022JB024131.
Raffi, I., Wade, B.S., Pälike, H., 2020. Chapter 29 - the Neogene Period. In: Gradstein, F. M., Ogg, J.G., Schmitz, M.D., Ogg, G.M. (Eds.), The Geologic Time Scale 2020, vol. 2. Elsevier, Boston, MA.
Repenning, C.A., Fejfar, O., Heinrich, W.D., 1990. Arvicolid rodent biochronology of the Northern Hemisphere. In: Fejfar, O., Heinrich Wolf, D. (Eds.), International Symposium on Evolution, Phylogeny and Biostratigraphy of Arvicolids (Rodentia, Mammalia). Geol. Survey, Prague, pp. 385–418.
Rodríguez-López, J.P., Liesa, C.L., van Dam, J., Lafuente, P., Arlegui, L., Ezquerro, L., de Boer, P.L., 2012. Aeolian construction and alluvial dismantling of a fault-bounded intracontinental aeolian dune field (Teruel Basin, Spain); a continental perspective on late Pliocene climate change and variability. Sedimentol. 59, 1536–1567.
Rohling, E.J., 1999. Environmental control on Mediterranean salinity and $\delta^{18}O$. Paleoceanogr. 14, 706–715.
Rohling, E.J., Yu, J., Heslop, D., Foster, G.L., Opdyke, B., Roberts, A.P., 2021. Sea level and deep- sea temperature reconstructions suggest quasi-stable states and critical transitions over the past 40 million years. Sci. Adv. 7, eabf5326. https://doi.org/10.1126/sciadv.abf5326.
Rosenzweig, M.L., McCord, R.D., 1991. Incumbent replacement: evidence for long-term evolutionary progress. Paleobiol. 17, 202–213.

Rossignol-Strick, M., 1985. Mediterranean Quaternary sapropels, an immediate response to African monsoons to variations of insolation. Palaeogeogr. Palaeoclimatol. Palaeoecol. 49, 237–263.
Ruddiman, W.F., Raymo, M.E., Martinson, D.G., Clement, B.M., Backman, J., 1989. Pleistocene evolution of Northern Hemisphere climate. Paleoceanogr. 4, 353–412.
Schmittner, A., Gruber, N., Mix, A.C., Key, R.M., Tagliabue, A., Westberry, T.K., 2013. Biology and air-sea gas exchange controls on the distribution of carbon isotope ratios ($\delta^{13}C$) in the ocean. Biogeosci. 10, 5793–5816.
Seltzer, A.M., Blard, P.-H., Sherwood, S.C., Kageyama, M., 2023. Terrestrial amplification of past, present, and future climate change. Sci. Adv. 9, eadf8119. https://doi.org/10.1126/sciadv.adf8119.
Sepkoski, J.J., 1996. Competition in macroevolution: The double wedge revisited. In: Jablonski, D., Erwin, D.H., Lipps, J.H. (Eds.), Evolutionary Paleobiology. Chicago University Press, Chicago, pp. 211–255.
Shackleton, N.J., Hall, M.A., 1997. The late Miocene stable isotope record, Site 926. In: Shackleton, N.J., Curry, W.B., Richter, C., Bralower, T.J. (Eds.), Proc. Ocean Drill. Program Sci. Res 154. Ocean Drill. Program, College Station, Texas, pp. 367–373.
Shackleton, N.J., Hall, M.A., Pate, D., 1995. Pliocene stable isotope stratigraphy of site 846. In: Proc. Ocean Drill. Program Sci. Res. 138. Ocean Drill. Program, College Station, Texas, pp. 337–355.
Short, D.A., Mengel, J.G., Crowley, T.J., Hyde, W.T., North, G.R., 1991. Filtering of Milankovitch cycles by Earth's geography. Quat. Res. 35, 157–173.
Sierro, F.J., Ledesma, S., Flores, J.-A., Torrescusa, S., del Olmo, W.M., 2000. Sonic and gamma-ray astrochronology: cycle to cycle calibration of Atlantic climatic records to Mediterranean sapropels and astronomical oscillations. Geology 28, 695–698.
Sinitsa, M.V., Čermák, S., Kryuchkova, L.Y., 2022. Cranial anatomy of *Csakvaromys bredai* (Rodentia, Sciuridae, Xerinae) and implications for ground squirrel evolution and systematics. J. Mamm. Evol. 29, 149–189.
Speijer, R.P., Pälike, H., Hollis, C.J., Hooker, J.J., Ogg, J.G., 2020. The Paleogene Period. In: Gradstein, F.M., Ogg, J.G., Schmitz, M.D., Ogg, G. (Eds.), Geological time scale 2020. Elsevier, Amsterdam, pp. 1087–1140.
Turco, E., Hilgen, F.J., Lourens, L.J., Shackleton, N.J., Zachariasse, W.J., 2001. Punctuated evolution of global climate cooling during the late Middle to early late Miocene: High-resolution planktonic foraminiferal and oxygen isotope records from the Mediterranean. Paleoceanogr. 16, 405–423.
Tzanova, A., Herbert, T.D., 2015. Regional and global significance of Pliocene Sea surface temperatures from the Gulf of Cadiz (Site U1387) and the Mediterranean. Glob. Planet. Chang. 133, 371–377.
Tzanova, A., Herbert, T.D., Peterson, L., 2015. Cooling Mediterranean Sea surface temperatures during the late Miocene provide a climate context for evolutionary transitions in Africa and Eurasia. Earth Planet. Sci. Lett. 419, 71–80.
Tzedakis, P.C., 2007. Seven ambiguities in the Mediterranean palaeoenvironmental narrative. Quat. Sci. Rev. 26, 2042–2066.
Valero, L., Garcés, M., Cabrera, L., Costa, E., Sáez, A., 2014. 20 Myr of eccentricity paced lacustrine cycles in the Cenozoic Ebro Basin. Earth Planet. Sci. Lett. 408, 183–193.
Valero, L., Cabrera, L., Sáez, A., Garcés, M., 2016. Long-period astronomically-forced terrestrial carbon sinks. Earth Planet. Sci. Lett. 444, 131–138.
Valla, P.G., van der Beek, P.A., Shuster, D.L., Braun, J., Herman, F., Tassan-Got, L., Gautheron, C., 2012. Late Neogene exhumation and relief development of the Aar and Aiguilles Rouges massifs (Swiss Alps) from low-temperature thermochronology modeling and $^4He/^3He$ thermochronometry. J. Geophys. Res. 117, F01004. https://doi.org/10.1029/2011JF002043.
van Balen, R.T., Forzoni, A., van Dam, J.A., 2015. Active faulting and folding along Jumilla Fault Zone, northeastern Betics. Spain. Geomorphol 237, 88–97.
van Dam, J.A., 1997. The small mammals from the upper Miocene of the Teruel-Alfambra region (Spain): paleobiology and paleoclimatic reconstructions. Geol. Ultraiect. 156, 1–204.
van Dam, J.A., 2006. Geographic and temporal patterns in the late Neogene (12-3 Ma) aridification of Europe: the use of small mammals paleoprecipitation proxies. Palaeogeogr. Palaeoclimatol. Palaeoecol. 238, 190–218.
van Dam, J.A., Reichart, G.J., 2009. Oxygen and carbon isotope signatures in late Neogene horse teeth from Spain and application as temperature and seasonality proxies. Palaeogeogr. Palaeoclimatol. Palaeoecol. 274, 64–81.
van Dam, J.A., Utescher, T., 2016. Plant- and micromammal-based paleoprecipitation proxies: comparing results of the Coexistence and Climate-Diversity Approach. Palaeogeogr. Palaeoclimatol. Palaeoecol. 443, 18–33.
van Dam, J.A., Alcalá, L., Alonzo Zarza, A., Calvo, J.P., Garcés, M., Krijgsman, W., 2001. The upper Miocene mammal record from the Teruel-Alfambra region (Spain). The MN system and continental stage/age concepts discussed. J. Vertebr. Paleontol. 21, 367–385.
van Dam, J.A., Abdul Aziz, H., Álvarez Sierra, M.Á., Hilgen, F.J., van den Hoek Ostende, L.W., Lourens, L.J., Mein, P., van der Meulen, A.J., Peláez-Campomanes, P., 2006. Long-period astronomical forcing of mammal turnover. Nature 443, 687–691.
van Dam, J.A., Furió, M., van Balen, R.T., 2014. Re-interpreting the biochronology of the La Celia and Los Gargantones mammal sites (late Miocene, Murcia, Spain). Geobios 47, 155–164.
van Dam, J.A., Mein, P., Garcés, M., van Balen, R.T., Furió, M., Alcalá, L., 2023. A new rodent chronology for the late Neogene of Spain. Geobios 76, 53–74.
van de Weerd, A., 1976. Rodent faunas of the Mio-Pliocene continental sediments of the Teruel-Alfambra region, Spain. Utrecht Micropaleontol. Bull. Spec. Publ. 2, 1–185.
van de Weerd, A., Daams, R., 1978. Quantitative composition of rodent faunas in the Spanish Neogene and paleoecological implications. Proc. K. Ned. Akad. Wet. Ser. B 81, 448–473.
van der Laan, E., Hilgen, F.J., Lourens, L.J., de Kaenel, E., Gaboardi, S., Iaccarino, S., 2012. Astronomical forcing of Northwest African climate and glacial history during the late Messinian (6.5-5.5 Ma). Palaeogeogr. Palaeoclimatol. Palaeoecol. 313, 107–126.
van der Meulen, M.J., Kouwenhoven, T.J., van der Zwaan, G.J., Meulenkamp, J.E., Wortel, M.J.R., 1999. Late Miocene uplift in the Romagnan Apennines and the detachment of subducted lithosphere. Tectonophys. 315, 319–335.
van der Schee, M., Sierro, F.J., Jiménez-Espejo, F.J., Hernández-Molina, F.J., Flecker, R., Flores, J.A., Acton, G., Gutjahr, M., Grunert, P., García-Gallardo, Á., Andersen, N., 2016. Evidence of early bottom water current flow after the Messinian Salinity Crisis in the Gulf of Cadiz. Mar. Geol. 380, 315–329.
Vrba, E.S., 1995. On the connections between paleoclimate and evolution. In: Vrba, E.S., Denton, G.H., Partridge, T.C., Burckle, L.H. (Eds.), Paleoclimate and Evolution, with Emphasis on Human Origins. Yale University, New Haven, pp. 24–45.
Wang, P.X., Tian, J., Lourens, L.J., 2010. Obscuring of long eccentricity cyclicity in Pleistocene oceanic carbon isotope records. Earth Planet. Sci. Lett. 290, 319–330.
Westerhold, T., Bickert, U., Röhl, U., 2005. Middle to late Miocene oxygen isotope stratigraphy of ODP site 1085 (SE Atlantic): new constrains on Miocene climate variability and sea-level fluctuations. Palaeogeogr. Palaeoclimatol. Palaeoecol. 217, 205–222.
Westerhold, T., Marwan, N., Drury, A.J., Liebrand, D., Agnini, C., Anagnostou, E., Barnet, J.S.K., Bohaty, S.M., De Vleeschouwer, D., Florindo, F., Frederichs, T., Hodell, D.A., Holbourn, A.E., Kroon, D., Lauretano, V., Littler, K., Lourens, L.J., Lyle, M., Pälike, H., Röhl, U., Tian, J., Wilkens, R.H., Wilson, P.A., Zachos, J.C., 2020. An astronomically dated record of Earth's climate and its predictability over the last 66 million years. Science 369, 1383–1387.
Zachos, J., Pagani, M., Sloan, L., Thomas, E., Billups, K., 2001a. Trends, rhythms, and aberrations in global climate 65 Ma to present. Science 292, 686–693.
Zachos, J., Shackleton, N.J., Revenaugh, J.S., Pälike, H., Flower, B.P., 2001b. Climate response to orbital forcing across the Oligocene-Miocene boundary. Science 292, 274–278.
Zagwijn, W.H., 1992. The beginning of the ice age in Europe and its major subdivisions. Quat. Sci. Rev. 11, 583–591.
Zhang, J., Quay, P.D., Wilbur, D.O., 1995. Carbon isotope fractionation during gas-water exchange and dissolution of CO_2. Geochim. Cosmochim. Acta 59, 107–114.